HHS Public Access

Author manuscript

Cell Rep. Author manuscript; available in PMC 2023 October 23.

Published in final edited form as:

Cell Rep. 2023 June 27; 42(6): 112615. doi:10.1016/j.celrep.2023.112615.

Pancreatic islet protection at the expense of secretory function involves serine-linked mitochondrial one-carbon metabolism

Angela Pelligra[1,9], **Jessica Mrugala**[1,2,3,9], **Kerstin Griess**[1,9], **Philip Kirschner**[1], **Oliver Nortmann**[1], **Barbara Bartosinska**[1], **Andrea Köster**[1], **Natalia I. Krupenko**[4], **Dominik Gebel**[1], **Philipp Westhoff**[5,6], **Bodo Steckel**[7], **Daniel Eberhard**[1,2], **Diran Herebian**[8], **Bengt-Frederik Belgardt**[2,3], **Jürgen Schrader**[7], **Andreas P.M. Weber**[5,6], **Sergey A. Krupenko**[4], **Eckhard Lammert**[1,2,3,10,*]

[1]Institute of Metabolic Physiology, Heinrich Heine University, 40225 Düsseldorf, Germany

[2]Institute for Vascular and Islet Cell Biology, German Diabetes Center (DDZ), Leibniz Center for Diabetes Research at Heinrich Heine University, 40225 Dusseldorf, Germany

[3]German Center for Diabetes Research (DZD e.V.), Helmholtz Zentrum München, 85764 Neuherberg, Germany

[4]University of North Carolina (UNC) Nutrition Research Institute, UNC Chapel Hill, Chapel Hill, NC, USA

[5]Institute of Plant Biochemistry, Cluster of Excellence on Plant Science (CEPLAS), Heinrich Heine University, 40225 Düsseldorf, Germany

[6]Cluster of Excellence on Plant Science (CEPLAS), Heinrich Heine University, 40225 Düsseldorf, Germany

[7]Department of Molecular Cardiology, Heinrich Heine University, 40225 Düsseldorf, Germany

[8]Department of General Pediatrics, Neonatology and Pediatric Cardiology, Medical Faculty and University Hospital Düsseldorf, Heinrich Heine University, 40225 Düsseldorf, Germany

[9]These authors contributed equally

[*]Correspondence: lammert@hhu.de.

AUTHOR CONTRIBUTIONS

A.P., J.M., and K.G. designed, performed, analyzed, and interpreted most of the experiments. P.K. helped with fluorescence-activated cell sorting, insulin secretion assays, and immunoblot analysis during the revision, and O.N. performed the initial *Atf4* KD experiments. D.G. helped to establish the generation of pseudo-islets from mouse islets. P.W. performed and analyzed gas chromatography-mass spectrometry (GC-MS) data for flux analysis. B.S. performed and analyzed UPLC data. D.H. performed and analyzed liquid chromatography-tandem mass spectrometry (LC-MS/MS) data for *db/db* plasma DXO concentrations. N.I.K., S.A.K., D.E., B.F.B., J.S., and A.W. provided scientific and experimental advice and methodology. D.E. performed controls of data integrity and analyses. E.L. supervised and scientifically guided A.P., J.M., K.G., and O.N. throughout the study. E.L. and K.G. wrote the manuscript with help from A.P. and J.M., who prepared the figures, schematic illustrations, legends, and methods to get her with K.G. and E.L. All authors read and revised the manuscript.

DECLARATION OF INTERESTS

E. L. declares the following competing financial interests: the author is an inventor of the US patent 10,464,904 entitled “Dextrorphan—derivatives with suppressed central nervous activity” and the US patent 9,370,511 entitled “Morphinan—derivatives for treating diabetes and related disorders.”

SUPPLEMENTAL INFORMATION

Supplemental information can be found online at https://doi.org/10.1016/j.celrep.2023.112615.

[10]Lead contact

SUMMARY

Type 2 diabetes is characterized by insulin hypersecretion followed by reduced glucose-stimulated insulin secretion (GSIS). Here we show that acute stimulation of pancreatic islets with the insulin secretagogue dextrorphan (DXO) or glibenclamide enhances GSIS, whereas chronic treatment with high concentrations of these drugs reduce GSIS but protect islets from cell death. Bulk RNA sequencing of islets shows increased expression of genes for serine-linked mitochondrial one-carbon metabolism (OCM) after chronic, but not acute, stimulation. In chronically stimulated islets, more glucose is metabolized to serine than to citrate, and the mitochondrial ATP/ADP ratio decreases, whereas the NADPH/$NADP^+$ ratio increases. Activating transcription factor-4 (Atf4) is required and sufficient to activate serine-linked mitochondrial OCM genes in islets, with gain- and loss-of-function experiments showing that Atf4 reduces GSIS and is required, but not sufficient, for full DXO-mediated islet protection. In sum, we identify a reversible metabolic pathway that provides islet protection at the expense of secretory function.

In brief

Pelligra et al. find that chronic exposure to high doses of K_{ATP}-dependent insulin secretagogues protects islets from cell death at the expense of secretory function. Dysfunctional islets upregulate serine-linked OCM genes and glucose flux to serine. Simultaneous knockdown of serine-linked mitochondrial OCM genes enhances insulin secretion but decreases islet viability.

Graphical Abstract:

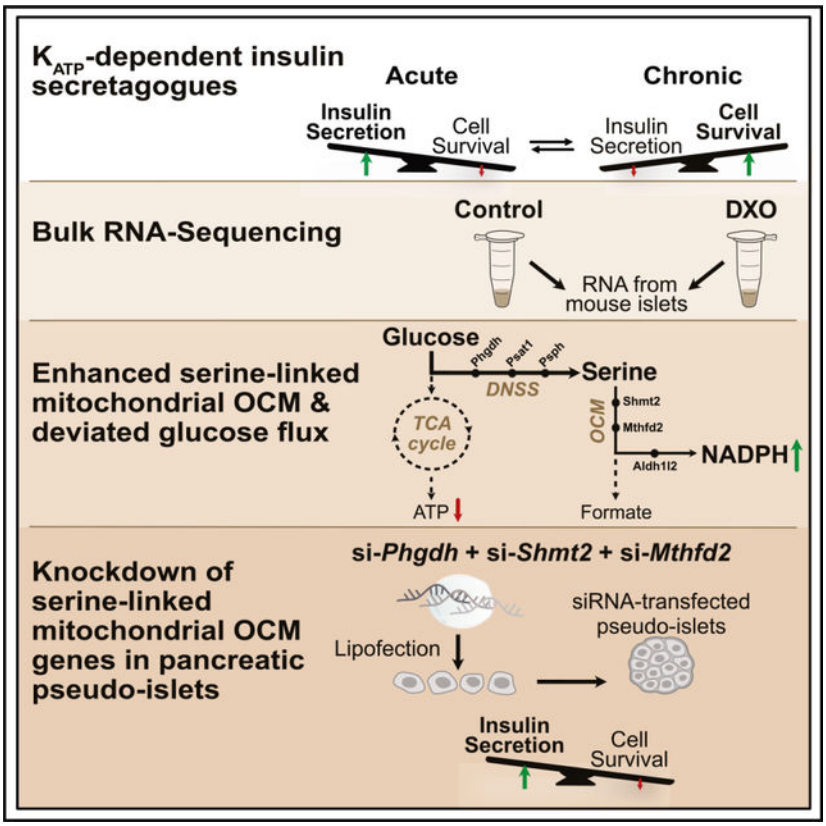

INTRODUCTION

Diabetes mellitus is a metabolic human disease characterized by elevated blood glucose concentrations due to insufficient insulin secretion and/or insulin resistance.[1]

Many diabetic patients require drug treatment to maintain normal blood glucose levels.[2] Metformin is the first-line medication,[3,4] but its strong anti-diabetic effect is reduced over time, making it necessary to use additional anti-diabetic drugs.[4–6] With few exceptions, most second-line medications for diabetes treatment enhance insulin secretion from pancreatic islets; these include sulfonylureas (such as glibenclamide) and incretin mimetics (such as exendin-4).[2,7] However, despite, or even due to these insulin secretagogues, pancreatic islet function often decreases, making replacement of islet secretory function with insulin injections inevitable for many patients with type 2 diabetes (T2D).[2]

The molecular mechanisms that drive islet dysfunction are not fully understood. In the past, at least three different, although not mutually exclusive, mechanisms have been suggested,[8] i.e., pancreatic beta cell death,[9,10] pancreatic beta cell de- or trans-differentiation into progenitor or non-beta cells,[11,12] and chronic endoplasmic reticulum (ER) stress combined with oxidative stress in pancreatic beta cells.[8,13–16]

Although T2D was considered incurable for a long time, recent studies using drastic interventions, such as bariatric surgery or extreme caloric restriction to lower insulin

demand, showed that islet secretory function (or GSIS) can be sufficiently restored to cure the disease at least in a subgroup of patients.[16–20] Previously, dextrorphan (DXO), the active metabolite of the cough suppressant dextromethorphan (DXM, the orally available prodrug of DXO), was found to increase GSIS via interaction with N-methyl-D-aspartate receptors (NMDARs) and ATP-sensitive potassium channels (K_{ATP} channels).[21] DXO also protected mouse and human pancreatic islets from cell death,[21–23] pointing to its potential as a second-line medication for the treatment of T2D. Further, in type 2 diabetic *db/db* mice, DXM was shown to delay onset of T2D and to substantially reduce blood glucose concentrations and islet cell death.[22] Moreover, it was shown that glutamate activates NMDARs on pancreatic beta cells and that deletion or pharmacologic inhibition of NMDARs enhances both GSIS and islet cell viability.[24,25] Notably, two registered randomized clinical trials (RCTs) in patients with T2D demonstrated that “acute,” single-dose treatment with DXM for 1 h increases postprandial plasma insulin concentrations and lowers blood glucose excursions in a following oral glucose tolerance test.[26]

In stark contrast to the positive reports on acute treatment, a previous small clinical trial showed that “chronic” treatment of four patients with very high doses of DXM (5- to 30-fold higher than used in the two single-dose RCTs) resulted in a reversible insulin-dependent diabetes mellitus (IDDM) in two of the patients, with blood glucose concentrations being higher than 300 mg/dL already after 48 h of drug treatment in one of the patients.[27] In this context, it is noteworthy that although treatment with sulfonylureas (such as glibenclamide) lowers blood glucose concentrations in individuals with T2D, chronic treatment of patients with these drugs can lead to islet dysfunction.[28,29] In addition, it was reported that human islets transplanted into the anterior eye chamber of mice developed signs of islet dysfunction when treated daily with a GLP-1R agonist for more than 200 days.[13]

Here we report that acute treatment (1 h) of islets with high concentrations of DXO (10 μM) enhances GSIS but does not affect islet cell survival. In contrast, chronic treatment (48 h) with 10 μM DXO or 1 μM glibenclamide leads to insulin secretory dysfunction, as characterized by reduced GSIS, but confers islet cell protection from cell death induced by streptozotocin (STZ) as a diabetogenic trigger. STZ was shown to induce oxidative stress and DNA damage in pancreatic beta cells,[30–32] which have been reported both in T2D mouse models as well as in islets from human donors with T2D.[33] The drug treatment lengths of 1 h (taken as acute treatment) and 48 h (taken as chronic treatment) were chosen, since the previous clinical trials with DXM showed that a 1 h treatment increased GSIS and blood glucose control, whereas a 48 h treatment with a high dose of DXM lowered insulin release and resulted in a reversible IDDM. Notably, in the *in vitro* experiments we developed, both the insulin secretory dysfunction and islet cell protection were reversible, as shown by the withdrawal of the insulin secretagogue DXO. To study this reversible islet phenotype, we used transcriptomic analyses after 24 h drug treatment (to observe changes in RNA levels at the onset of the developing islet phenotype) and metabolomic analyses as well as genetic manipulations after 48 h drug treatment (when the islet phenotype with less GSIS and more viability is fully developed) to identify serine-linked mitochondrial one-carbon metabolism (OCM) as the metabolic pathway associated with islet cell protection at the expense of insulin secretory function. Our findings on this metabolic pathway (which

has been largely unexplored in pancreatic islets) warrants further studies of this particular pathway during progression and drug treatment of human T2D.

RESULTS

Chronic exposure of islets to high concentrations of the insulin secretagogue DXO or glibenclamide protects from cell death at the expense of secretory function

We treated pancreatic islets with high concentrations of DXO (10 μM) for different times (i.e., 1 h and 48 h) and analyzed glucose-stimulated insulin secretion (GSIS) and islet cell survival after addition of streptozotocin (STZ) (Figures 1 and S1), a frequently used toxin to induce IDDM.[34,35] Acute (1 h) treatment with DXO was found to enhance GSIS at high glucose concentrations without altering basal insulin secretion or insulin content (Figures 1A and S1A), as previously reported.[22] Of note, this acute DXO treatment did not protect mouse pancreatic islets from STZ-induced cell death (Figure 1B).

In contrast to the acute treatment, opposite effects were observed after chronic exposure of islets to high concentrations of the drug. More specifically, treatment with 10 μM DXO for 48 h was found to decrease GSIS at high glucose concentrations and to reduce the insulin content (Figures 1C and S1B) but provided full protection of the pancreatic islets from STZ-induced cell death (Figure 1D). The cell-protective effects of DXO were demonstrated by applying two independent methods, i.e., (1) staining with ethidium homodimer-1 (EthD-1) followed by fluorescence microscopy and ImageJ/Fiji-based image analysis, and (2) flow cytometry analyses of dispersed islet cells treated with fixable viability stain (FVS) 660 (Figures 1B, 1D, and S1D). We also observed that the insulin secretory capacity was restored when the islets were transferred for 24 h to regular islet media (hence without the insulin secretagogue) (Figure 1E), even though the insulin content was not restored (Figure S1C). Notably, removal of DXO not only rescued the insulin secretory function of islets but also the DXO-mediated islet cell protection vanished (Figure 1F), revealing an inverse correlation between islet secretory function and islet cell survival.

Next, we investigated whether induction of the reversible islet secretory dysfunction in combination with islet cell protection could also be observed with other insulin secretagogues. Thus, islets were incubated with a high dose of glibenclamide, a K_{ATP} channel antagonist, and exendin-4, a GLP-1R agonist, for 48 h. Notably, 1 μM glibenclamide also led to an islet secretory dysfunction (i.e., reduced GSIS) and a lower insulin content as well as pronounced islet cell protection from STZ-mediated cell death (Figures S1E, S1G, and S1I). In stark contrast to DXO and glibenclamide, whose mechanisms of action (MOAs) depend on K_{ATP} channels, chronic treatment (for 48 h) with the GLP-1R agonist exendin-4 reduced neither the islet secretory function nor the insulin content of islets (Figures S1F and S1H) but also did not protect pancreatic islets from STZ-mediated cell death in this experimental setting (Figure S1J).

In sum, our results show that, depending on the drug, its concentration, and its treatment duration, pancreatic islets can switch from a state of high insulin secretion to a state of high islet cell protection.

Chronic exposure of islets to high concentrations of DXO or glibenclamide induces expression of genes for serine-linked mitochondrial OCM

To uncover the potential molecular mechanisms associated with islet cell protection at the expense of islet secretory function, we assessed differentially expressed genes in DXO-treated (10 μM) islets at the time point (24 h) when islet secretory dysfunction and cell protection developed (Figure 2A). RNA sequencing (RNA-seq) identified 698 genes to be differentially expressed upon chronic DXO treatment, representing 3.1% of all analyzed genes (Figure 2A). Strikingly, mRNAs of genes involved in the ER stress response, including *Activating transcription factor 4 (Atf4), DNA damage-inducible transcript 3 (Ddit3,* also known as *Chop), and Heat shock protein family A (Hsp70) member 5 (Hspa5*, also known as *Grp78* or *BiP*) were found to be upregulated after treatment with the insulin secretagogue (Figure 2B). Atf4 upregulation was subsequently validated at protein level by immunoblotting (Figures 2C and 2D). Furthermore, the DXO treatment increased expression of genes coding for enzymes in *de novo* serine biosynthesis via the phosphorylated pathway, i.e., *Phosphoglycerate dehydrogenase (Phgdh), Phosphoserine aminotransferase 1 (Psat1), and Phosphoserine phosphatase (Psph)* (Figure 2E). Immunoblot analysis demonstrated upregulation of Phgdh at the protein level (Figures 2F and 2G).

Three genes of the mitochondrial OCM, i.e., *Serine hydroxymethyltransferase 2 (Shmt2), Methylenetetrahydrofolate dehydrogenase 2 (Mthfd2) and Aldehyde dehydrogenase 1 family member L2 (Aldh1l2),* were also upregulated at the mRNA level (Figure 2H). In contrast, expression of genes coding for the cytosolic isoforms of these enzymes, i.e., *Shmt1*, *Mthfd1*, and *Aldh1l1*, was not altered (Figure 2H). To validate the upregulation of the mitochondrial enzyme Aldh1l2 at the protein level, pancreatic islets were fractionated into cytosolic and mitochondrial fractions and analyzed by immunoblotting. As expected, Aldh1l2 protein could only be detected in the mitochondrial fraction of the pancreatic islets, containing cytochrome *c* oxidase subunit 4 (Cox IV), and was elevated upon induction of islet dysfunction (Figure 2I, upper blot). Quantifications of immunoblots with pancreatic islet lysates, confirmed enhanced Aldh1l2 protein levels as well (Figure 2I, lower blot, and Figure 2J).

Consistent with the notion that chronic stimulation of insulin secretion could potentially dedifferentiate pancreatic islets,[12,36] the pancreatic beta cell marker genes *Insulin* (*Ins1, Ins2*), *Solute carrier family 2 member 2 (Slc2a2), MAF bZIP transcription factor A (MafA), and Pancreatic and Duodenal Homeobox-1 (Pdx1)* were significantly downregulated after DXO treatment (Figure S2A) but without affecting protein levels of Glut2 (encoded by *Slc2a2*) during the first 48 h of drug treatment (Figures S2B and S2C). Proliferation markers were found to be reduced as well, except for some weakly upregulated genes, such as *Cdc25a* and *Pcna* (Figure S2D). Notably, the selective NMDAR antagonist MK-801, whose MOA strictly depends on K_{ATP} channels,[22] altered RNA expression in a similar manner compared with the less selective NMDAR antagonist DXO (Figures S2E–S2I), including an upregulation of ER stress marker genes as well as genes involved in *de novo* serine synthesis and mitochondrial OCM (Figures S2E–S2G). In contrast to chronic treatment, acute treatment of islets with 10 μM DXO did not substantially change the above-mentioned RNAs (Figures S3A–S3D).

The effects of chronic DXO treatment on the islet expression of mRNAs for Atf4 and serine-linked mitochondrial OCM enzymes were found to be strictly dependent on the dose of DXO (Figures S3E–S3K). More specifically, at a concentration of 1 μM DXO or lower, not all of these genes were significantly higher in their mRNA expression, whereas, at 10 μM DXO, all of the mRNAs were robustly and significantly upregulated (Figures S3E–S3K). Further, the genes for insulin (*Ins1* and *Ins2*) were significantly downregulated only at a DXO concentration as high as 10 μM but not at a concentration of 1 μM or lower (Figures S3L and S3M). Consistent with these dose-dependent effects, chronic treatment of *db/db* mice with 3 mg/mL DXM, corresponding to a plasma concentration of 1 μM DXO (see Figure S4D), reduced (rather than accelerated) onset of T2D and islet cell demise, as revealed by lower blood glucose concentrations and a visibly more intact shape of the islets, respectively (Figures S4A–S4D). Of note, the body weight of the animals remained largely unchanged at the end of the study in the 3 mg/mL DXM group and 1 mg/mL DXM control group (Figure S4B), as previously reported.[22] Further, expression of the mRNAs for ER stress markers and serine-linked mitochondrial OCM were not consistently upregulated in the islets from DXM-treated *db/db* mice, suggesting that also *in vivo* a lower DXO concentration (1 μM) does not result in insulin secretory dysfunction, even when given for 2 weeks (Figures S4E–S4G). In addition, islet cell and proliferation markers were not consistently changed after treating *db/db* mice with 3 mg/mL DXM versus 1 mg/mL DXM in the drinking water (Figures S4H and S4I).

In vitro, we observed that spliced and hence activated Xbp-1s was detectable at a higher protein level in DXO-treated islets compared with untreated islets (Figures 3A and 3B), consistent with the reported induction by Xbp-1s of *Atf4* and *Fgf21* mRNA,[37–39] both of which were found to be upregulated in DXO-treated islets (Figure 2B). In support of the reversible nature of the observed gene signature, we could demonstrate that protein levels of Aldh1l2 and Atf4 decreased after washout of the insulin secretagogue DXO (Figure 3C). Similar results were obtained for *Atf4, Phgdh, Psat1*, *Psph*, *Shmt2*, *Mthfd2*, and *Aldh1l2* mRNAs, which returned to normal levels after washout (Figures 3D–3J). Consistent with the opposing effects of glibenclamide (acting via K_{ATP} channels like DXO) and exendin-4 (acting via GLP-1R) in chronically treated islets (Figure S1), glibenclamide enhanced the mRNA expression of Atf4, the enzymes for serine biosynthesis, and mitochondrial OCM to a larger extent than exendin-4 (Figure S5).

We conclude that chronic stimulation of pancreatic islets with high concentrations of the insulin secretagogues DXO (10 μM) or glibenclamide (1 μM) significantly increased expression of genes for serine-linked mitochondrial OCM, which were reported to promote cell proliferation and survival in other cell types,[40–44] and that the insulin secretagogue exendin-4 increased their expression to a lesser extent.

Chronic stimulation of pancreatic islets with DXO shifts the glycolytic flux toward products of serine-linked mitochondrial OCM

Our RNA-seq data indicated that chronic stimulation of pancreatic islets with high concentrations of the insulin secretagogue DXO shifted glucose metabolism from the tricarboxylic acid (TCA) cycle, needed for full ATP production and insulin secretory

function,[45,46] toward serine-linked mitochondrial OCM (Figure 4A), established to be involved in cell survival and cell division.[44,47] To explore such metabolic reprogramming, we performed stable isotope tracing experiments. For this purpose, we incubated pancreatic islets with [U-^{13}C]-glucose in the presence or absence of 10 μM DXO for 1 h or 48 h, mimicking acute or chronic drug exposure, respectively. The incorporation of ^{13}C atoms into metabolites was subsequently analyzed in (1) citrate as a product of the TCA cycle and (2) serine as a product of *de novo* serine synthesis (Figures 4B–4E). After 1 h of DXO treatment, no significant alterations in ^{13}C-labeled citrate and serine were observed (Figures 4B and 4C). In contrast, we detected less incorporation of ^{13}C atoms from glucose into citrate (M+1 to M+5) as well as more unlabeled citrate (M+0) upon chronic (48 h) DXO treatment, indicating that less glucose was metabolized via the TCA cycle (Figure 4D). Conversely, we observed higher incorporation of ^{13}C-labeled units from glucose into serine (M+1 and M+2) and less unlabeled serine (M+0) after 48 h of DXO treatment (Figure 4E; please note that one of the ^{13}C atoms gets lost during fragmentation). These findings are consistent with our results from RNA-seq, indicating that chronic treatment of islets with high concentrations of the insulin secretagogue DXO shifts the glycolytic flux from glycolysis and TCA cycle to *de novo* serine synthesis (Figure 4A).

Next, we wished to determine whether the expression of components for oxidative phosphorylation (OXPHOS) were altered by using several antibodies against mitochondrial proteins. However, no significant changes were identified (Figure S6), except for complex I (NDUFB8) and complex V (ATP5a) proteins, which were found to be increased in half of the islet preparations (Figures S6B and S6F). We then measured by using ultra-performance liquid chromatography (UPLC) the concentrations of NADH, NAD$^+$, ATP, ADP, and NADPH and NADP$^+$ in the mitochondrial fraction of mouse islets that were treated with or without DXO for 48 h. Consistent with the expected reduction in the TCA cycle activity (Figure 4A, left part of the illustration), the analysis revealed that DXO significantly decreased mitochondrial NADH/NAD$^+$ and ATP/ADP ratios (Figures 4F and 4G). In contrast, mitochondrial NADPH/NADP$^+$ ratios increased in pancreatic islets upon chronic DXO treatment (Figure 4H), indicating the activation of serine-linked mitochondrial OCM (Figure 4A, right part of the illustration).

Our data show that chronic (but not acute) stimulation of pancreatic islets with high concentrations of DXO activates serine-linked mitochondrial OCM (as judged by the increase in ^{13}C-labeled serine and mitochondrial NADPH/NADP$^+$ ratio), which is essential for coping with oxidative stress and cell survival. In turn, chronic treatment with DXO decreases the products of the TCA cycle and oxidative phosphorylation (i.e., ^{13}C-labeled citrate as well as mitochondrial NADH/NAD$^+$ and ATP/ADP ratios), which are necessary for physiologic insulin secretory function.

ATF4 expression in pseudo-islets is sufficient for limiting GSIS but not for islet cell protection

Previous studies have shown that upregulation of *Phgdh, Psat1*, and *Psph* (i.e., genes involved in *de novo* serine synthesis) as well as *Shmt2* and *Mthfd2* (genes involved in mitochondrial OCM) are dependent on the ER stress regulator Atf4.[47–50] In pancreatic islets,

the role of Atf4 is controversial, with reports suggesting positive as well as negative roles of Atf4 in islet cell survival.[41,51–53] Here, we investigated whether Atf4 is required for DXO-mediated islet secretory dysfunction, islet cell protection, or both.

To perform gain-of-function experiments, we first dispersed pancreatic islets into an islet cell suspension and subsequently infected the cells with a recombinant adenovirus carrying the human *ATF4* gene (Ad-ATF4) or *GFP* as a control (Ad-*GFP*). Afterward, pseudo-islets were generated by a hanging drop method,[54,55] allowing analyses of the effects of ATF4 expression in primary islet cells in three-dimensional islets (Figure 5A). *ATF4* mRNA was successfully overexpressed in infected pseudo-islets (Figure 5B). Upon *ATF4* expression, the pseudo-islets showed an upregulation of *Phgdh*, *Psat1*, and *Psph* mRNAs, i.e., all parts of *de novo* serine synthesis (via the phosphorylated pathway), as well as of *Shmt2*, *Mthfd2*, and *Aldh1l2* mRNAs, i.e., elements of the mitochondrial OCM (Figures 5F–5H). In addition, immunoblot analyses confirmed expression of ATF4 as well as upregulation of Phgdh and Aldh1l2 at the protein level (Figure 5I).

We then performed a GSIS assay with *Ad-GFP* and *Ad-ATF4* infected pseudo-islets and observed a reduced GSIS and enhanced insulin content upon *ATF4* expression (Figures 5J and 5K), which is in line with DXO-induced Atf4 affecting negatively GSIS. To study whether ATF4 also mediated the islet cell protection against STZ, we evaluated cell viability by flow cytometry (Figure 5L). As already visible in bright-field images (Figure 5M), this analysis did not reveal any change in the untreated pseudo-islets, whereas more cell death was detected in the ATF4-expressing pseudo-islets (94.72%) compared with control islets (80.85%) after STZ treatment (Figures 5L and 5M). These results show that the ATF4 expression mimics DXO-induced upregulation of serine-linked mitochondrial OCM genes and the DXO-induced islet secretory dysfunction but does not simulate the beta cell-protective effect of DXO.

Atf4 is required for limiting GSIS and required for full islet protection from STZ-induced cell death

To complement the gain-of-function experiments, we performed loss-of-function experiments to explore whether silencing *Atf4* could increase GSIS and/or decrease islet cell viability. We knocked down *Atf4* in pseudo-islets by small interfering RNA (siRNA) before the DXO treatment (Figure 6A). Levels of *Atf4* mRNA were efficiently reduced in these experiments (Figure 6B). Notably, *Atf4* knockdown in pseudo-islets was sufficient to reduce the DXO-mediated induction of genes for the *de novo* serine synthesis and mitochondrial OCM pathways (Figures 6C–6H). In addition, the silencing of *Atf4* strongly lowered Atf4 and Aldh1l2 protein expression (Figure 6I), and this effect was more pronounced in pseudo-islets treated with the ER stress inducer thapsigargin (Figure 6I).

Finally, we assessed the effect of DXO on GSIS in *Atf4*-proficient and *Atf4*-silenced pseudo-islets. The *Atf4* knockdown was found to increase GSIS (Figure 6J) but to decrease the islet insulin content (Figure 6K). Notably, DXO-mediated islet cell protection from STZ-induced cell death was significantly attenuated by Atf4 knockdown (Figures 6L and 6M), while basal and STZ-induced cell death were similar between pseudo-islets transfected with control and *Atf4* siRNAs (Figures 6L and 6M). Consistent with a requirement for Atf4

in DXO-mediated upregulation of serine-linked OCM, isotope tracing experiments showed that DXO induced the conversion of glucose into serine (at the expense of citrate) to a lesser extent when *Atf4* had been silenced in pseudo-islets (Figures S7A and S7B). In contrast, DXO-mediated beta cell dedifferentiation was found to be unaffected by the knockdown of *Atf4* (Figures S7C–S7H).

We conclude that Atf4 is required in pancreatic islets for (1) induction of genes for serine-linked mitochondrial OCM, (2) limiting islet secretory function, and (3) full DXO-mediated islet protection from STZ-induced cell death.

Serine-linked mitochondrial OCM is required for limiting GSIS and required for full islet protection from STZ-induced cell death

To determine whether the enzymes of serine-linked mitochondrial OCM are involved in insulin secretion and islet cell viability, we performed knockdown experiments in pseudo-islets for *Phgdh* (Figures 7A–7C), *Shmt2* (Figures 7D–7F), and *Mthfd2* (Figures 7G–7I), with the knockdown validated at the protein level in each case. We also performed triple knockdown experiments in which all three genes, i.e., *Phgdh*, *Shmt2*, and *Mthfd2*, were silenced (Figures 7J–7L). We observed that each individual knockdown increased GSIS from pancreatic pseudo-islets, demonstrating that each of the three genes for serine-linked mitochondrial OCM is required to limit GSIS (Figures 7B, 7E, and 7H). Knockdown of all three genes led to the highest increase in GSIS (Figure 7K), compared with the knockdown of each gene alone (Figures 7B, 7E, and 7H). Of note, knockdown of each single gene did not affect the viability of islets after incubation with STZ (Figures 7C, 7F, and 7I), while the triple knockdown of *Phgdh*, *Shmt2*, and *Mthfd2* enhanced the STZ-induced islet cell death (Figure 7L). Even though knockdown of these genes did not fully attenuate the effects of chronic high-dose DXO treatment, the data show that each of the three genes involved in serine-linked mitochondrial OCM is required for limiting GSIS, while all three genes (*Phgdh*, *Shmt2*, and *Mthfd2*) are essential to fully protect pancreatic islets from STZ-mediated cell death.

DISCUSSION

T2D is often associated with insulin resistance, which increases the demand for pancreatic islets to secrete large amounts of insulin to maintain blood glucose concentrations at physiological levels. Insulin secretagogues, such as sulfonylureas and NMDAR antagonists (both acting via K_{ATP} channels), as well as GLP-1R agonists that we used in this study, stimulate GSIS. However, excessive insulin biosynthesis and secretion are thought to potentially contribute to islet secretory dysfunction (or reduced GSIS) at some point during the disease.[16] Here we established an *in vitro* model for the development of insulin secretory dysfunction by stimulating mouse pancreatic islets with a high concentration of the insulin secretagogue DXO (an NMDAR antagonist). A similar insulin secretory dysfunction could be induced by stimulation of islets with glibenclamide (a K_{ATP} blocker) but not by exposure of islets to exendin-4 (a GLP-1R agonist). In our study, we demonstrated that the DXO-induced secretory dysfunction is connected to a strong upregulation of the transcription factor Atf4 as well as expression of several serine-linked mitochondrial (but not cytosolic)

OCM genes. We further showed that Atf4 is required and sufficient to induce expression of these genes in pancreatic islets, including the gene for Aldh1l2.

Our data are consistent with previous reports on cell lines unrelated to pancreatic islets showing that ATF4 is a master regulator of genes involved in serine biosynthesis and mitochondrial OCM.[47–50,56] They are also consistent with studies on glucolipotoxicity induced by stimulation of islets with high glucose and palmitate concentrations where coincidently some alterations in serine-linked OCM genes were observed.[57–59] It is therefore possible that serine-linked mitochondrial OCM plays a universal role in T2D, which is reversible to some extent. In addition, a role of folate and OCM has been previously implicated in beta cell differentiation, underscoring the key role of this evolutionarily conserved pathway in pancreatic islets.[60]

This study is the first to show that the genes for key enzymes of this metabolic pathway are significantly turned on upon continuous stimulation of islets with two insulin secretagogues that both act via K_{ATP} channels. On the one hand, upregulated expression of serine-linked mitochondrial OCM genes is reversible and associated with insulin secretory dysfunction as well as reduced mitochondrial NADH/NAD^+ and ATP/ADP ratios. On the other hand, we show that, at the time when pancreatic islets develop an insulin secretory dysfunction and dedifferentiate, the islets are protected from cell death induced by the beta cell toxin STZ and have elevated mitochondrial NAPDH/$NADP^+$ ratios. It is noteworthy that our findings are consistent with the observation that serine is essential for mitochondrial biology and cell survival, as this amino acid is involved in mitochondrial redox regulation, nutrient utilization, and production of ceramides.[61,62] Further, the first-line medication of T2D, metformin, was shown to have positive effects on pancreatic islets from humans with T2D,[9] and metformin inhibits the activity of the mitochondrial OCM enzyme SHMT2, but not that of its cytosolic form, SHMT1.[63]

In sum, serine-linked mitochondrial OCM is strongly but reversibly turned on upon chronic stimulation with high concentrations of insulin secretagogues, which act via K_{ATP} channels, whereas it is only weakly activated upon stimulation with GLP-1R agonists (i.e., exendin-4). Our study further demonstrated that, in pancreatic islets, serine-linked mitochondrial OCM genes are upregulated by ATF4. Our findings explain why chronic treatment of patients with high concentration of NMDAR antagonists or sulfonylureas triggers an insulin secretory dysfunction even though our knockdown experiments cannot explain the chronic effects with an upregulation of these serine-linked mitochondrial OCM genes alone. Finally, the reported inverse correlation between insulin secretory function and islet protection points to the intrinsic difficulty of chronically stimulating insulin secretion with K_{ATP}-dependent insulin secretagogues, further underscoring the notion that, compared with these drugs, GLP-1R-based insulin secretagogues (which only weakly activate this metabolic pathway) are better suited for the treatment of T2D when administered chronically and at a high dose.

Limitations of the study

For the specific analysis of the serine-linked OCM, it was not possible to perform experiments in cell culture models such as INS1E cells. In immortalized tumor cells, this specific pathway is of fundamental importance to cope with oxidative stress occurring in

rapidly proliferating cells. Therefore, it was not possible to conduct experiments in cell culture.

STAR★METHODS

RESOURCE AVAILABILITY

Lead contact—Further information and request for resources and reagents should be directed to and will be fulfilled by the lead contact Dr. Eckhard Lammert (lammert@hhu.de).

Materials availability—This study did not generate new unique reagents. There are restrictions to the availability of Aldh1l2 antibody used in this study due to discontinued production by the company.

Data and code availability

- RNA-sequencing data were deposited on Mendeley database at "Pelligra et al. 2023" and are publicly available as of the date of publication. DOIs are listed in the key resources table. Mendeley Data: https://data.mendeley.com/datasets/4rwmrc9cpr and https://data.mendeley.com/datasets/g4bdvw6czr. Original immunoblot images are shown in Data S1. All other data such as Microscopy, UPLC and MS-data reported in this paper will be shared by the lead contact upon request.
- The code for pancreatic islet analyses is the same like in the paper of Scholz et al.,[64] and has been deposited at Zenodo. DOI is listed in the key resources table.
- Any additional information required to reanalyze the data reported in this paper is available from the lead contact upon request

EXPERIMENTAL MODEL AND STUDY PARTICIPANT DETAILS

Mouse models—For *in vitro* experiments only male mice of the lines, C57BL/6J (Janvier) (of the age of 9–11 week), C57BL/6NTac (Taconic) (of the age of 9–11 week), and BKS(D)-*Lepr*^{db}/JOrlRj (*db/db*) (Janvier) (of the age of 4–6 weeks) were used. All mice were kept in constantly monitored housing conditions (22°C, 55% humidity, 12:12 h light:dark cycle) and had unlimited access to standard laboratory rodent chow and water. All animal experiments were approved by the local Animal Ethics Committee of the Landesamt für Natur, Umwelt und Verbraucherschutz Nordrhein-Westfalen (LANUV, North Rhine-Westphalia, Germany) and conducted according to the German Animal Protection Laws.

METHOD DETAILS

Chronic DXM treatment of *db/db* mice—Chronic *in vivo* effects of DXM on pancreatic islets were investigated on four-weeks-old *db/db* mice, which were treated for 2 weeks with DXM (Sigma-Aldrich). Therefore, DXM was administered via drinking water at 1 mg/mL vs. 3 mg/mL DXM concentrations. Fasting blood glucose (BG) levels and body weights (BW) were controlled weekly in mice. Blood glucose was measured from the tail tip, using the GlucoSmart Swing2 glucometer and corresponding test strips (MSP

Bodmann GmbH). For the quantification of DXO plasma concentrations, additional blood was collected and used for tandem mass spectrometry (LC-MS/MS). After two weeks of treatment, mice were sacrificed for isolation of islets, which were immediately used for RNA-isolation and RNA-Seq.

Isolation of murine pancreatic islets—All *in vitro* experiments were performed on isolated pancreatic mouse islets. The isolation was performed according to Yesil et al.[65] with minor changes. Pancreata were excised after *papilla vateri* occlusion and perfusion with Dulbecco's modified eagle medium (DMEM) + GlutaMAX (1 g/mL glucose) (Gibco by Life Technologies) containing Liberase TL Research Grade (Roche) through the bile duct. The enzymatic digestion was stopped after 16.5 min at 37°C with DMEM containing 15% heat-inactivated Fetal Bovine Serum (FBS, Gibco by Life Technologies). After washing, filtration, and gradient centrifugation at 1,200 g for 25 min using Histopaque-1077 (Sigma-Aldrich) or Lymphoprep (STEMCell Technologies), the isolated islets were collected from the interphase between DMEM and density gradient medium and transferred into islet medium. Islet medium is composed of Connaught Medical Research Laboratories (CMRL) 1066 medium (Gibco by Life Technologies) supplemented with 15% heat-inactivated FBS, 100 U/ml penicillin (Gibco by Life Technologies), 100 µg/mL streptomycin (Gibco by Life Technologies), 50 µM β-mercaptoethanol (Gibco by Life Technologies), 0.15% sodium bicarbonate (Gibco by Life Technologies), and 10 mM glucose (Sigma-Aldrich). Islets were washed twice in islet medium and cultured in a humidified incubator at 37°C and 5% CO_2. All treatments and functional assays within this study were performed after overnight cultivation.

Pseudo-islet generation—Overnight cultured isolated islets were washed several times in Dulbecco's Phosphate Buffered Saline (DPBS, Gibco by Life Technologies) and digested with 0.05% Trypsin-EDTA (Gibco by Life Technologies) to obtain a single-cell suspension. Once the islets were fully dissociated, the enzymatic digestion reaction was stopped with islet medium. The number of viable cells was determined using trypan blue (0.4%, Gibco by Life Technologies) staining. For the generation of pseudo-islets, hanging drop technology was performed according to the previously described protocol[54] with minor changes. Therefore, single cells were resuspended in islet medium at a density of 1500 cells/30 µL and distributed in 30 µL drops on the lids of petri-dishes containing 25 mL DPBS. Hanging drops were incubated for 3 days in a humidified incubator at 37°C and 5% CO_2 to form pseudo-islets. Afterward, pseudo-islets were collected in islet media and used for functional analyses.

Adenovirus transduction in mouse pancreatic islets—For efficient overexpression of ATF4 in pancreatic islets, dispersed islet cells were infected for 6 h in a humidified incubator at 37°C and 5% CO_2 with a multiplicity of infection (MOI) of 200 with adenoviruses containing either a human ATF4 overexpression plasmid (Vector Biolabs, # ADV-201618, RefSeq: BC011994, further designated as Ad-*ATF4*) or a GFP control plasmid (ViraQuest Inc., VQAd CMV eGFP, further designated as Ad-*GFP*), followed by the formation of pseudo-islets by hanging drop technique. For this, islet cells were washed with islet media, resuspended at a density of 1500 cells/30 µL and hanging drops were

pipetted to generate pseudoislets within 3 days. Previous to conduction of functional assays, pseudo-islets were washed several times with islet medium and the absence of infectious particles in the islet medium was ensured by performing a PCR against the adenovirus plasmid construct.

siRNA-mediated gene knockdown in mouse pancreatic islets—Gene knockdown was conducted using Lipofectamine RNAiMAX Transfection Reagent (Thermo Fisher Scientific). For this purpose, non-targeting control siRNA (Horizon Discovery, # D-001810-10-50) or siRNAs targeting specific genes of interest was mixed with Lipofectamine and OptiMEM (Gibco by Life Technologies), incubated for 5 min at room temperature, and added with a final concentration of 50 nM to dispersed islet cells to a density of 1500 cells/30 μL. Pseudo-islets were generated by hanging drop technique and collected for further treatments and assays after 3 days of incubation at 37°C and 5% CO_2. See Table S2 for the used siRNAs (Horizon Discovery)

Glucose-stimulated insulin secretion assay—Functionality of islet cells, deriving from C57BL/6J and C57BL/6NTac mice was studied upon dextrorphan tartrate (DXO, Sigma-Aldrich, #D127, solved in H_2O) treatment. All treatments were performed at 37°C and 5% CO_2 in islet medium containing 10 mM glucose with different incubation periods. Duration of pre-incubation and concentrations are indicated in the figures. To investigate basal and glucose-stimulated insulin secretion (GSIS) levels, an insulin secretion assay was performed. Previous to stimulation with low and high glucose concentrations, 8 islets were washed twice and starved for 1 h in Krebs Ringer HEPES (KRH) buffer containing 15 mM HEPES (Gibco by Life Technologies), 5 mM KCl (Chemsolute, Th.Geyer), 120 mM NaCl (Carl Roth), 2 mM $CaCl_2$ (Sigma-Aldrich), 10 μM glycine (Sigma-Aldrich), 24 mM $NaHCO_3$ (Sigma-Aldrich), 0.1% Bovine Serum Albumin (BSA, Sigma-Aldrich) and 2 mM glucose (Sigma-Aldrich). All incubation steps were performed at 37°C and 5% CO_2. In order to measure the basal- and glucose-stimulated insulin secretion, the starved islets were successively incubated for 1 h in KRH buffer containing 2 mM (low glucose), followed by an additional 1 h of incubation in 20 mM (high glucose). Subsequent to each stimulation, supernatants containing the secreted insulin were collected. Finally, islets were lysed in radioimmunoprecipitation assay (RIPA) buffer (50 mM Tris-HCl, pH 7.4 (Sigma-Aldrich), 150 mM NaCl (Roth), 1 mM EDTA (Ambion), 1 mM Na_3VO_4 (Sigma-Aldrich), 1 mM NaF (Sigma-Aldrich), 0.25% Sodium deoxycholate (AppliChem), 1% IGEPAL (Sigma-Aldrich) in H_2O), to measure insulin content. The amount of secreted insulin as well as insulin content was determined using the ultra-sensitive rat insulin ELISA (Crystal Chem) according to manufacturer's instructions. The colorimetric readout was carried out using the Infinite M200 NanoQuant reader (Tecan) or GloMax Discover Microplate Reader (Promega).

RNA isolation from mouse pancreatic islets—For RNA-sequencing analysis and quantification of gene expression levels in mouse pancreatic islets, total RNA was extracted from pancreatic islets using the RNeasy Mini Kit (Qiagen). Cultured islets were transferred and washed in ice-cold PBS, lysed in RLT lysis buffer (Qiagen) and used for RNA isolation according to manufacturer's instruction. To obtain pure RNA, genomic DNA contaminations

were removed by an on-column DNase digestion, using the RNase-Free DNase Set (Qiagen). RNA concentration and quality was measured using BioMate 3 (Thermo Fisher Scientific).

RNA-sequencing—To investigate downstream target genes of DXO in pancreatic islets, whole transcriptome analysis was performed via RNA-sequencing at the Functional Genomics Center Zurich (FGCZ, ETH in Zurich, Switzerland). The quality of the RNA was determined with Qubit (2.0) Fluorometer (Life Technologies, California, USA) and a TapeStation 4200 RNA Screen Tape (Agilent, Waldbronn, Germany). RNA integrity number (RIN) values were above 9.1 for all samples, and a Poly-A enrichment strategy for generating sequencing libraries was chosen. RNA samples with RIN >9.1 were pooled from three independent experiments (see Figure 2A). For the succeeding steps, the TruSeq mRNA Stranded Library Prep Kit (Illumina, Inc, California, USA) was used. After Poly-A selection using Oligo-dT beads, the mRNA was reverse-transcribed into complementary DNA (cDNA). The cDNA samples were fragmented, end-repaired and polyadenylated before ligation of TruSeq UD Indices (IDT, Coralville, Iowa, USA). Fragments were selectively amplified with PCR. The quality and quantity of the enriched libraries were validated using Qubit (1.0) Fluorometer and TapeStation 4200 D1000 Screen Tape (Agilent, Waldbronn, Germany). For cluster generation, the TruSeq SR Cluster kit HS4000 (Illumina, Inc, California, USA) was used. Next, 10 pM of pooled normalized libraries were used on the cBOT System. The library sequencing was performed on the HiSeq4000 with 125 cycles single-read using the TruSeq SBS Kit HS4000 (Illumina, Inc, California, USA). RNA-Sequencing reads were aligned to the mouse GRCm38 reference genome using the STAR aligner.[66] Gene expression values were computed with the function featureCounts from the R package Rsubread.[67] Differential expression was computed using the generalized linear model implemented in the Bioconductor package edgeR.[68] Expression values were indicated as the metric “fragments per kilobase of transcript per million mapped reads” (FPKM). The Sushi framework was used to run the data analyses.[69] Genes were only considered expressed if the FPKM value was above >1. For further analysis the cutoff for the log2 Fold Change (log2 FC) was set above >1 or below < −1, and a false discovery rate (FDR) of less than 0.05 was considered significant.

Reverse transcriptase PCR and quantitative real-time PCR—Quantitative real-time PCR was conducted to determine gene expression on mRNA level. RNA was transcribed to complementary DNA (cDNA) using the SuperScriptII reverse transcriptase (Invitrogen by Thermo Fisher Scientific) or High-Capacity cDNA Reverse Transcription Kit (Invitrogen by Thermo Fisher Scientific). Subsequently, qPCR was performed using the FastStart Essential Green Master-Mix (Roche) or LUNA Universal (RT)-qPCR reagent (NEB). See Table S2 for the used oligonucleotides sequences (Eurogentec).

qPCR was performed utilizing the LightCycler Nano Device (Roche) with the LightCycler Nano software 1.1. 2, the QuantStudio 1 system (Applied Biosystems) or QuantStudio 7 Flex Real-Time PCR System with the Quantstudio Design Analysis Desktop Software. Calculation of $2^{-\Delta CT}$ was performed by the comparative C_T method, in which ΔC_T is

defined as C_T gene of interest – C_T reference gene. All data were normalized to the expression levels of the housekeeping genes *Beta-actin* and *Hprt* and to the control.

Fractionation of pancreatic islets—To analyze the localization of Aldh1l2 upon DXO treatment islets were fractionated using the Mitochondria/Cytosol Fractionation Kit (Abcam, ab65320). 120–150 islets were treated and homogenized according to manufacturer's instructions. After collecting the cytosolic fraction, the mitochondrial protein lysate was obtained by resuspending the pellet in 100 μL mitochondrial extraction buffer. Localization was detected via immunoblot analysis.

Immunoblot analysis—To investigate and quantify protein expression, 20–80 islets per sample were washed in ice-cold PBS, homogenized in RIPA buffer containing a cocktail of protease inhibitors (Roche) and placed on a cell disrupter at 4°C for 10 min. 4x Laemmli buffer (BioRad) containing 40 mM NaF (Sigma-Aldrich), and 4% β-mercaptoethanol (Roth), was added to samples and boiled for 5–10 min at 95°C. Protein lysates serving for OXPHOS immunoblots were not boiled. Polypeptides and protein ladder (Precision Plus Protein Dual Color (BioRad) or PageRuler Pre-stained (Thermo)) were separated using 4–15% pre-cast Mini-Protean TGX Stain-free Protein Gels (Bio-Rad) and blotted on polyvinylidine difluoride (PVDF) membranes using the Trans-Blot Turbo Transfer System (Bio-Rad). Subsequent to a blocking step of 1–2 h at room temperature with 5% bovine serum albumin (BSA) (AppliChem) or 5% non-fat dried milk (Roth) dissolved in PBS ±0.1% Tween 20 (AppliChem), the membranes were incubated overnight at 4°C with specific mono- or polyclonal antibodies. Following washing with PBS ±0.1% Tween 20, the membranes were incubated for 1 h at room temperature with an appropriate horseradish peroxidase (HRP)-conjugated secondary antibody anti-rabbit or anti-mouse antibody. See Table S1 for the used primary and secondary antibodies. For detection, the Clarity Western ECL substrate (Bio-Rad) was used according to manufacturer's instructions. The images were acquired using the ChemiDoc XRS (Bio-Rad) or ChemiDoc MP Imaging System (BioRad), while the protein quantification was performed using Fiji[70] (ImageJ) or Image Lab (Bio-Rad) analysis software. The amount of protein in each sample was normalized to the housekeeper Beta-actin or for adenoviral experiments to GFP expression.

Measurement of islet cell viability in mouse islets and pseudo-islets via microscopy—Islet cell viability of mouse pancreatic islets and pseudo-islets was examined upon 1.5 mM STZ treatment for 24 h, using the LIVE-DEAD Viability-Cytotoxicity Kit (Thermo Fisher Scientific). Following treatment, whole islets were incubated protected from light for 1 h at 37°C and 5% CO_2 with 10 μg/mL Hoechst 33342 (DNA stain), 2 μM Calcein AM (live cells), and 4 μM Ethidium homodimer-1 (EthD-1, dead cells) in KRH buffer supplemented with 0.1% BSA (Sigma-Aldrich) and 10 mM glucose (Sigma-Aldrich) to co-stain cell nuclei, as well as viable and dead cells. Afterward, Z-stack images of the stained islets were acquired using a Zeiss LSM 710 coupled to an Axio Observer.Z1 microscope (Carl Zeiss MicroImaging GmbH) equipped with a Plan-Apochromat 20x/0.8 objective or Zeiss ApoTome (Carl Zeiss MicroImaging GmbH) equipped with a Plan-Apochromat 103/0.45 objective. All images were analyzed using Fiji (ImageJ) image analysis software and cell death was quantified by using the

semi-automated quantification macro as previously published by Scholz and colleagues.[64] The area of dead (EthD-1-positive) cells of each islet was normalized to the whole islet cell area (Hoechst-positive).

Measurement of islet cell viability in pseudo-islets via flow cytometry—For flow cytometric analyses of cell viability, 80–100 pseudo-islets per condition were treated for 24 h with 2.5 mM STZ in a 6-well dish. Afterward, islet cell media and dispersed islets were transferred to FACS tubes, centrifuged for 5 min at 400 g and washed with PBS. Subsequently, islet cells were stained with FVS660 (1:1,000 in PBS, BD Biosciences) for 15 min at room temperature in the dark, adenovirus infected pseudo-islets were additionally fixed with 4% PFA for 30 min at room temperature, and washed again with PBS. Finally, the amount of FVS660-positive (FL4-H positive, dead) and FVS660-negative (FL4-H negative, living) beta cells was determined using the FACSCalibur (BD Biosciences) or CytoFlex S (Beckmann Coulter). Quantification was conducted using FlowJo software version 10 (BD Biosciences).

GC-MS flux analysis of ^{13}C-labeled metabolites—For metabolic flux analysis, 100–300 pseudo- or pancreatic mouse islets per condition were initially pre-incubated for 48 h in normal or 10 mM [U-^{13}C]-Glucose (Sigma, 389374) containing islet media. Thereafter, islets were transferred in respective islet media with or without 10 μM DXO supplementation for additional 1 h–48 h. Afterward, islet were washed three times with ice-cold isotonic NaCl solution and processed for metabolite extraction according to Arrivault et al. with minor changes.[71] Metabolite analysis was conducted using a 7890B gas chromatography system connected to a 7200 QTOF mass spectrometer (Agilent Technologies) as previously described.[72] The software MassHunter Qualitative (v b08, Agilent Technologies) was used for compound identification by comparing mass spectra to an in-house library of authentic standards and to the NIST14 Mass Spectral Library (https://www.nist.gov/srd/nist-standard-reference-database-1a-v14). Peak areas were integrated using MassHunter Quantitative (v b08, Agilent Technologies) and normalized to the internal standard ribitol (Sigma, A5502). To determine the ^{13}C incorporation, the fragment *m/z* 204 (C_2 fragment) was used for serine and the fragment *m/z* 273 (C_5 fragment) for citrate. For both fragments, the potential isotopologues were evaluated. The normalized peak areas were corrected for the natural abundance using the R package IsoCorrectoR.[73]

LC-MS/MS analysis of DXO in plasma—DXO concentration in blood plasma of 1 mg/mL vs. 3 mg/mL DXM treated *db/db* mice was quantified as previously described by Scholz et al.[64] In brief, mouse plasma samples including deuterated internal standard d_3-dextrorphan (d_3-DXO, Sigma-Aldrich) were analyzed by ultra-pressure liquid chromatography coupled to tandem mass spectrometry (UPLC-MS/MS). The UPLC-I Class and the tandem mass spectrometer Xevo-TQS (Waters) were used for the analysis. DXO was separated on an Acquity UPLC BEH C18 column (1.7 μm, 100 mm × 2.1 mm, Waters). The column oven temperature was 40°C, the flow rate 0.4 mL/min, and the injection volume was 2 μL. The first mobile phase A consists of 5 mM ammonium acetate including 0.05% formic acid, while the second mobile phase B consists of acetonitrile. An isocratic elution mode

(A:B, 65:35) was applied. Tandem mass spectrometric analysis was performed in positive electrospray ionization mode. Multiple reaction monitoring (MRM) mode with following mass transitions were applied: m/z: 258 > 157 (DXO) and 261 > 157 (d_3-DXO). Collision energy of 40 V and 30 V were used for fragmentation of DXO/d_3-DXO.

UPLC—For quantification of intra-mitochondrial ATP/ADP, NADPH/$NADP^+$ and NADH/NAD^+ ratios, Ultra Performance Liquid Chromatographic (UPLC) analyses were performed at 17°C. 400 pancreatic mouse islets were pre-treated for 48 h either with 10 μM DXO in islet medium or without DXO, as control. Thereafter, islets were washed in 1 mL ice-cold 0.9% NaCl solution and fractionated using the Mitochondria/Cytosol Fractionation Kit (Abcam, ab65320). For purine extraction, mitochondria were lysed by resuspending the pellet in 100 μL ice-cold lysis-buffer (22.25% ddH_2O, 22.25% chloroform, 55.5% methanol). After centrifugation (15 min, 21,000 g, 4°C) the supernatant, containing mitochondrial analytes, was collected, vacuum-dried, and resuspended in 50 μL Hanks' Balanced Salt Solution (HBSS) at room temperature. UPLC analyses were performed according to Aplak et al. using Waters Acquity Ultra Performance Liquid Chromatographic System Bio H class.[74] For purine analysis, a sample volume of 40 μL was injected by a cooling autosampler on a Cortecs C18+ UPLC column (3.0 × 150 mm, 1.6 μM) (Waters Corp.; Milford, MA, USA). Separation was performed by running a linear gradient of buffer A (200 mM KH_2PO_4/200 mM KCl, at pH 6) and buffer B (200 mM KH_2PO_4/200 mM KCl/7.5% acetonitrile (v/v) at pH 6) with a flow profile of 0.340 mL/min as followed: initial 100% A; 0.03 min 96% A, 4% B; 4.53 min 91% A, 9% B; 22.63 min 5% A, 95% B; 26.10 min 5% A, 95% B; 26.50 min 100% A. For detection of analytes a Waters TUV Detector Module at 254 nm was used. After each run, the column was washed and thereby re-equilibrated using buffer A (100%) at a flow rate of 0.34 mL/min for 8 min.

QUANTIFICATION AND STATISTICAL ANALYSIS

All statistical analyses were performed with GraphPad Prism 9 software (RRID:SCR_002798) and conducted as indicated in the figure legends. Depending on the experimental design, different statistical tests were conducted. Thus, p values between two related groups were calculated by an unpaired two-tailed student's t test or a paired two-tailed student's t test, while multiple group conditions were evaluated by either One- or two-way ANOVA, followed by Dunnett's, or Tukey's-comparison analysis. If not otherwise indicated, all data were shown as mean ± standard error of the mean (SEM). Microscopical analyses of cell viability were conducted under blinded conditions as well as UPLC and GC-MS flux analysis. In glucose-stimulated insulin secretion- and cell viability assays, single significant outliers (p value ≤0.05), detected by Grubbs' test for outliers, were excluded. For both methods, only experiments with significant GSIS induction + DXO exhaustion or significant STZ cell death induction + DXO protection in control treatments were evaluated. Number of replicates and reproductions are given in the figure legends.

Supplementary Material

Refer to Web version on PubMed Central for supplementary material.

ACKNOWLEDGMENTS

We thank N. Klöcker and A. Reichert for experimental advice, as well as Y. Koh for schematic illustrations. This study was supported by the Deutsche Forschungsgemeinschaft (DFG) through the research training group RTG 2576 ("vivid – *In vivo* investigations towards the early development of type 2 diabetes"), the Federal Ministry of Health, and the Ministry of Culture and Science of North Rhine-Westphalia. Metabolite analyses were supported by the CE-PLAS Plant Metabolism and Metabolomics Laboratory, which is funded by the DFG under Germany's Excellence Strategy (EXC-2048/1; project ID 390686111). S.A.K. is supported by NIH grant DK117854.

REFERENCES

1. Chatterjee S, Khunti K, and Davies MJ (2017). Type 2 diabetes. Lancet 389, 2239–2251. 10.1016/s0140-6736(17)30058-2. [PubMed: 28190580]
2. Welters A, Klüppel C, Mrugala J, Wörmeyer L, Meissner T, Mayatepek E, Heiss C, Eberhard D, and Lammert E (2017). NMDAR antagonists for the treatment of diabetes mellitus-Current status and future directions. Diabetes Obes. Metabol. 19, 95–106. 10.1111/dom.13017.
3. He L (2020). Metformin and systemic metabolism. Trends Pharmacol. Sci. 41, 868–881. 10.1016/j.tips.2020.09.001. [PubMed: 32994049]
4. Welters A, and Lammert E (2014). Diabetes mellitus. In Metabolism of Human Diseases: Organ Physiology and Pathophysiology (Springer).
5. Turner RC, Cull CA, Frighi V, and Holman RR (1999). Glycemic control with diet, sulfonylurea, metformin, or insulin in patients with type 2 diabetes mellitus: progressive requirement for multiple therapies (UKPDS 49). UK Prospective Diabetes Study (UKPDS) Group. JAMA 281, 2005–2012. 10.1001/jama.281.21.2005. [PubMed: 10359389]
6. Kahn SE, Haffner SM, Heise MA, Herman WH, Holman RR, Jones NP, Kravitz BG, Lachin JM, O'Neill MC, Zinman B, et al. (2006). Glycemic durability of rosiglitazone, metformin, or glyburide monotherapy. N. Engl. J. Med. 355, 2427–2443. 10.1056/NEJMoa066224. [PubMed: 17145742]
7. Idris I, and Donnelly R (2007). Dipeptidyl peptidase-IV inhibitors: a major new class of oral antidiabetic drug. Diabetes Obes. Metabol. 9, 153–165. 10.1111/j.1463-1326.2007.00705.x.
8. Swisa A, Glaser B, and Dor Y (2017). Metabolic stress and compromised identity of pancreatic beta cells. Front. Genet. 8, 21. 10.3389/fgene.2017.00021. [PubMed: 28270834]
9. Marchetti P, Del Guerra S, Marselli L, Lupi R, Masini M, Pollera M, Bugliani M, Boggi U, Vistoli F, Mosca F, and Del Prato S (2004). Pancreatic islets from type 2 diabetic patients have functional defects and increased apoptosis that are ameliorated by metformin. J. Clin. Endocrinol. Metab. 89, 5535–5541. 10.1210/jc.2004-0150. [PubMed: 15531508]
10. Butler AE, Janson J, Bonner-Weir S, Ritzel R, Rizza RA, and Butler PC (2003). Beta-cell deficit and increased beta-cell apoptosis in humans with type 2 diabetes. Diabetes 52, 102–110. 10.2337/diabetes.52.1.102. [PubMed: 12502499]
11. Cinti F, Bouchi R, Kim-Muller JY, Ohmura Y, Sandoval PR, Masini M, Marselli L, Suleiman M, Ratner LE, Marchetti P, and Accili D (2016). Evidence of beta-cell dedifferentiation in human type 2 diabetes. J. Clin. Endocrinol. Metab. 101, 1044–1054. 10.1210/jc.2015-2860. [PubMed: 26713822]
12. Talchai C, Xuan S, Lin HV, Sussel L, and Accili D (2012). Pancreatic beta cell dedifferentiation as a mechanism of diabetic beta cell failure. Cell 150, 1223–1234. 10.1016/j.cell.2012.07.029. [PubMed: 22980982]
13. Abdulreda MH, Rodriguez-Diaz R, Caicedo A, and Berggren PO (2016). Liraglutide compromises pancreatic beta cell function in a humanized mouse model. Cell Metabol. 23, 541–546. 10.1016/j.cmet.2016.01.009.
14. Zraika S, Aston-Mourney K, Laybutt DR, Kebede M, Dunlop ME, Proietto J, and Andrikopoulos S (2006). The influence of genetic background on the induction of oxidative stress and impaired insulin secretion in mouse islets. Diabetologia 49, 1254–1263. 10.1007/s00125-006-0212-9. [PubMed: 16570159]
15. Retnakaran R, Kramer CK, Choi H, Swaminathan B, and Zinman B (2014). Liraglutide and the preservation of pancreatic beta-cell function in early type 2 diabetes: the LIBRA trial. Diabetes Care 37, 3270–3278. 10.2337/dc14-0893. [PubMed: 25249651]

16. van Raalte DH, and Verchere CB (2016). Glucagon-like peptide-1 receptor agonists: beta-cell protection or exhaustion? Trends Endocrinol. Metabol. 27, 442–445. 10.1016/j.tem.2016.04.009.

17. Guidone C, Manco M, Valera-Mora E, Iaconelli A, Gniuli D, Mari A, Nanni G, Castagneto M, Calvani M, and Mingrone G (2006). Mechanisms of recovery from type 2 diabetes after malabsorptive bariatric surgery. Diabetes 55, 2025–2031. 10.2337/db06-0068. [PubMed: 16804072]

18. Purnell JQ, Selzer F, Wahed AS, Pender J, Pories W, Pomp A, Dakin G, Mitchell J, Garcia L, Staten MA, et al. (2016). Type 2 diabetes remission rates after laparoscopic gastric bypass and gastric banding: results of the longitudinal assessment of bariatric surgery study. Diabetes Care 39, 1101–1107. 10.2337/dc15-2138. [PubMed: 27289123]

19. Taylor R (2021). Type 2 diabetes and remission: practical management guided by pathophysiology. J. Intern. Med. 289, 754–770. 10.1111/joim.13214. [PubMed: 33289165]

20. Kahn SE, Cooper ME, and Del Prato S (2014). Pathophysiology and treatment of type 2 diabetes: perspectives on the past, present, and future. Lancet 383, 1068–1083. 10.1016/S0140-6736(13)62154-6. [PubMed: 24315620]

21. Gresch A, and Düfer M (2020). Dextromethorphan and dextrorphan influence insulin secretion by interacting with KATP and L-type Ca(2+) channels in pancreatic beta-cells. J. Pharmacol. Exp. Therapeut. 375, 10–20. 10.1124/jpet.120.265835.

22. Marquard J, Otter S, Welters A, Stirban A, Fischer A, Eglinger J, Herebian D, Kletke O, Klemen MS, Stožer A, et al. (2015). Characterization of pancreatic NMDA receptors as possible drug targets for diabetes treatment. Nat. Med. 21, 363–372. 10.1038/nm.3822. [PubMed: 25774850]

23. Wollheim CB, and Maechler P (2015). Beta cell glutamate receptor antagonists: novel oral antidiabetic drugs? Nat. Med. 21, 310–311. 10.1038/nm.3835. [PubMed: 25849270]

24. Huang XT, Yue SJ, Li C, Huang YH, Cheng QM, Li XH, Hao CX, Wang LZ, Xu JP, Ji M, et al. (2017). A sustained activation of pancreatic NMDARs is a novel factor of beta-cell apoptosis and dysfunction. Endocrinology 158, 3900–3913. 10.1210/en.2017-00366. [PubMed: 28938426]

25. Huang XT, Li C, Peng XP, Guo J, Yue SJ, Liu W, Zhao FY, Han JZ, Huang YH, Yang L, et al. (2017). An excessive increase in glutamate contributes to glucose-toxicity in beta-cells via activation of pancreatic NMDA receptors in rodent diabetes. Sci. Rep. 7, 44120. 10.1038/srep44120. [PubMed: 28303894]

26. Marquard J, Stirban A, Schliess F, Sievers F, Welters A, Otter S, Fischer A, Wnendt S, Meissner T, Heise T, and Lammert E (2016). Effects of dextromethorphan as add-on to sitagliptin on blood glucose and serum insulin concentrations in individuals with type 2 diabetes mellitus: a randomized, placebo-controlled, double-blinded, multiple cross-over, single-dose clinical trial. Diabetes Obes. Metabol. 18, 100–103. 10.1111/dom.12576.

27. Konrad D, Sobetzko D, Schmitt B, and Schoenle EJ (2000). Insulin-dependent diabetes mellitus induced by the antitussive agent dextromethorphan. Diabetologia 43, 261–262. 10.1007/s001250050042. [PubMed: 10753054]

28. Rosengren A, Jing X, Eliasson L, and Renström E (2008). Why treatment fails in type 2 diabetes. PLoS Med. 5, e215. 10.1371/journal.pmed.0050215. [PubMed: 18959474]

29. Remedi MS, and Nichols CG (2008). Chronic antidiabetic sulfonylureas in vivo: reversible effects on mouse pancreatic beta-cells. PLoS Med. 5, e206. 10.1371/journal.pmed.0050206. [PubMed: 18959471]

30. Jain D, Weber G, Eberhard D, Mehana AE, Eglinger J, Welters A, Bartosinska B, Jeruschke K, Weiss J, Päth G, et al. (2015). DJ-1 protects pancreatic beta cells from cytokine- and streptozotocin-mediated cell death. PLoS One 10, e0138535. 10.1371/journal.pone.0138535. [PubMed: 26422139]

31. Xue J, Scotti E, and Stoffel M (2019). CDK8 regulates insulin secretion and mediates postnatal and stress-induced expression of neuropeptides in pancreatic beta cells. Cell Rep. 28, 2892–2904.e7. 10.1016/j.celrep.2019.08.025. [PubMed: 31509750]

32. Bolzán AD, and Bianchi MS (2002). Genotoxicity of streptozotocin. Mutat. Res. 512, 121–134. 10.1016/s1383-5742(02)00044-3. [PubMed: 12464347]

33. Tornovsky-Babeay S, Dadon D, Ziv O, Tzipilevich E, Kadosh T, Schyr-Ben Haroush R, Hija A, Stolovich-Rain M, Furth-Lavi J, Granot Z, et al. (2014). Type 2 diabetes and congenital

hyperinsulinism cause DNA double-strand breaks and p53 activity in beta cells. Cell Metabol. 19, 109–121. 10.1016/j.cmet.2013.11.007.

34. Lenzen S (2008). The mechanisms of alloxan- and streptozotocin-induced diabetes. Diabetologia 51, 216–226. 10.1007/s00125-007-0886-7. [PubMed: 18087688]
35. Lenzen S (2008). Oxidative stress: the vulnerable beta-cell. Biochem. Soc. Trans. 36, 343–347. 10.1042/BST0360343. [PubMed: 18481954]
36. Okamoto H, Hribal ML, Lin HV, Bennett WR, Ward A, and Accili D (2006). Role of the forkhead protein FoxO1 in beta cell compensation to insulin resistance. J. Clin. Invest. 116, 775–782. 10.1172/JCI24967. [PubMed: 16485043]
37. Zhang D, De Veirman K, Fan R, Jian Q, Zhang Y, Lei L, Evans H, Wang Y, Lei L, Wang B, et al. (2020). ER stress arm XBP1s plays a pivotal role in proteasome inhibition-induced bone formation. Stem Cell Res. Ther. 11, 516. 10.1186/s13287-020-02037-3. [PubMed: 33256835]
38. Wang T, Li LY, Chen YF, Fu SW, Wu ZW, Du BB, Yang XF, Zhang WS, Hao XY, and Guo TK (2021). Ribosome assembly factor URB1 contributes to colorectal cancer proliferation through transcriptional activation of ATF4. Cancer Sci. 112, 101–116. 10.1111/cas.14643. [PubMed: 32888357]
39. Jiang S, Yan C, Fang QC, Shao ML, Zhang YL, Liu Y, Deng YP, Shan B, Liu JQ, Li HT, et al. (2014). Fibroblast growth factor 21 is regulated by the IRE1alpha-XBP1 branch of the unfolded protein response and counteracts endoplasmic reticulum stress-induced hepatic steatosis. J. Biol. Chem. 289, 29751–29765. 10.1074/jbc.M114.565960. [PubMed: 25170079]
40. Gao S, Ge A, Xu S, You Z, Ning S, Zhao Y, and Pang D (2017). PSAT1 is regulated by ATF4 and enhances cell proliferation via the GSK3beta/beta-catenin/cyclin D1 signaling pathway in ER-negative breast cancer. J. Exp. Clin. Cancer Res. 36, 179. 10.1186/s13046-017-0648-4. [PubMed: 29216929]
41. Kitakaze K, Oyadomari M, Zhang J, Hamada Y, Takenouchi Y, Tsuboi K, Inagaki M, Tachikawa M, Fujitani Y, Okamoto Y, and Oyadomari S (2021). ATF4-mediated transcriptional regulation protects against beta-cell loss during endoplasmic reticulum stress in a mouse model. Mol. Metabol. 54, 101338. 10.1016/j.molmet.2021.101338.
42. Quirós PM, Prado MA, Zamboni N, D'Amico D, Williams RW, Finley D, Gygi SP, and Auwerx J (2017). Multi-omics analysis identifies ATF4 as a key regulator of the mitochondrial stress response in mammals. J. Cell Biol. 216, 2027–2045. 10.1083/jcb.201702058. [PubMed: 28566324]
43. Wortel IMN, van der Meer LT, Kilberg MS, and van Leeuwen FN (2017). Surviving stress: modulation of ATF4-mediated stress responses in normal and malignant cells. Trends Endocrinol. Metabol. 28, 794–806. 10.1016/j.tem.2017.07.003.
44. Yang M, and Vousden KH (2016). Serine and one-carbon metabolism incancer. Nat. Rev. Cancer 16, 650–662. 10.1038/nrc.2016.81. [PubMed: 27634448]
45. Maechler P, and Wollheim CB (2001). Mitochondrial function in normal and diabetic beta-cells. Nature 414, 807–812. 10.1038/414807a. [PubMed: 11742413]
46. Barsby T, and Otonkoski T (2022). Maturation of beta cells: lessons from in vivo and in vitro models. Diabetologia 65, 917–930. 10.1007/s00125-022-05672-y. [PubMed: 35244743]
47. Ye J, Mancuso A, Tong X, Ward PS, Fan J, Rabinowitz JD, and Thompson CB (2012). Pyruvate kinase M2 promotes de novo serine synthesis to sustain mTORC1 activity and cell proliferation. Proc. Natl. Acad. Sci. USA 109, 6904–6909. 10.1073/pnas.1204176109. [PubMed: 22509023]
48. Adams CM (2007). Role of the transcription factor ATF4 in the anabolic actions of insulin and the anti-anabolic actions of glucocorticoids. J. Biol. Chem. 282, 16744–16753. 10.1074/jbc.M610510200. [PubMed: 17430894]
49. DeNicola GM, Chen PH, Mullarky E, Sudderth JA, Hu Z, Wu D, Tang H, Xie Y, Asara JM, Huffman KE, et al. (2015). NRF2 regulates serine biosynthesis in non-small cell lung cancer. Nat. Genet. 47, 1475–1481. 10.1038/ng.3421. [PubMed: 26482881]
50. Ben-Sahra I, Hoxhaj G, Ricoult SJH, Asara JM, and Manning BD (2016). mTORC1 induces purine synthesis through control of the mitochondrial tetrahydrofolate cycle. Science 351, 728–733. 10.1126/science.aad0489. [PubMed: 26912861]

51. Shrestha N, De Franco E, Arvan P, and Cnop M (2021). Pathological beta-cell endoplasmic reticulum stress in type 2 diabetes: current evidence. Front. Endocrinol. 12, 650158. 10.3389/fendo.2021.650158.
52. Yusta B, Baggio LL, Estall JL, Koehler JA, Holland DP, Li H, Pipeleers D, Ling Z, and Drucker DJ (2006). GLP-1 receptor activation improves beta cell function and survival following induction of endoplasmic reticulum stress. Cell Metabol. 4, 391–406. 10.1016/j.cmet.2006.10.001.
53. Liew CW, Bochenski J, Kawamori D, Hu J, Leech CA, Wanic K, Malecki M, Warram JH, Qi L, Krolewski AS, and Kulkarni RN (2010). The pseudokinase tribbles homolog 3 interacts with ATF4 to negatively regulate insulin exocytosis in human and mouse beta cells. J. Clin. Invest. 120, 2876–2888. 10.1172/JCI36849. [PubMed: 20592469]
54. Cavallari G, Zuellig RA, Lehmann R, Weber M, and Moritz W (2007). Rat pancreatic islet size standardization by the “hanging drop” technique. Transplant. Proc. 39, 2018–2020. 10.1016/j.transproceed.2007.05.016. [PubMed: 17692680]
55. Kim HJ, Alam Z, Hwang JW, Hwang YH, Kim MJ, Yoon S, Byun Y, and Lee DY (2013). Optimal formation of genetically modified and functional pancreatic islet spheroids by using hanging-drop strategy. Transplant. Proc. 45, 605–610. 10.1016/j.transproceed.2012.11.014. [PubMed: 23498797]
56. Ye J, Fan J, Venneti S, Wan YW, Pawel BR, Zhang J, Finley LWS, Lu C, Lindsten T, Cross JR, et al. (2014). Serine catabolism regulates mitochondrial redox control during hypoxia. Cancer Discov. 4, 1406–1417. 10.1158/2159-8290.CD-14-0250. [PubMed: 25186948]
57. Cnop M, Abdulkarim B, Bottu G, Cunha DA, Igoillo-Esteve M, Masini M, Turatsinze JV, Griebel T, Villate O, Santin I, et al. (2014). RNA sequencing identifies dysregulation of the human pancreatic islet transcriptome by the saturated fatty acid palmitate. Diabetes 63, 1978–1993. 10.2337/db13-1383. [PubMed: 24379348]
58. Marselli L, Piron A, Suleiman M, Colli ML, Yi X, Khamis A, Carrat GR, Rutter GA, Bugliani M, Giusti L, et al. (2020). Persistent or transient human beta cell dysfunction induced by metabolic stress: specific signatures and shared gene expression with type 2 diabetes. Cell Rep. 33, 108466. 10.1016/j.celrep.2020.108466. [PubMed: 33264613]
59. Hall E, Volkov P, Dayeh T, Bacos K, Rönn T, Nitert MD, and Ling C (2014). Effects of palmitate on genome-wide mRNA expression and DNA methylation patterns in human pancreatic islets. BMC Med. 12, 103. 10.1186/1741-7015-12-103. [PubMed: 24953961]
60. Karampelias C, Rezanejad H, Rosko M, Duan L, Lu J, Pazzagli L, Bertolino P, Cesta CE, Liu X, Korbutt GS, and Andersson O (2021). Reinforcing one-carbon metabolism via folic acid/Folr1 promotes beta-cell differentiation. Nat. Commun. 12, 3362. 10.1038/s41467-021-23673-0. [PubMed: 34099692]
61. Gao X, Lee K, Reid MA, Sanderson SM, Qiu C, Li S, Liu J, and Locasale JW (2018). Serine availability influences mitochondrial dynamics and function through lipid metabolism. Cell Rep. 22, 3507–3520. 10.1016/j.celrep.2018.03.017. [PubMed: 29590619]
62. Locasale JW (2013). Serine, glycine and one-carbon units: cancer metabolism in full circle. Nat. Rev. Cancer 13, 572–583. 10.1038/nrc3557. [PubMed: 23822983]
63. Tramonti A, Cuyàs E, Encinar JA, Pietzke M, Paone A, Verdura S, Arbusà A, Martin-Castillo B, Giardina G, Joven J, et al. (2021). Metformin is a pyridoxal-5’-phosphate (PLP)-Competitive inhibitor of SHMT2. Cancers 13, 4009. 10.3390/cancers13164009. [PubMed: 34439169]
64. Scholz O, Otter S, Welters A, Wörmeyer L, Dolenšek J, Klemen MS, Pohorec V, Eberhard D, Mrugala J, Hamacher A, et al. (2021). Peripherally active dextromethorphan derivatives lower blood glucose levels by targeting pancreatic islets. Cell Chem. Biol. 28, 1474–1488. 10.1016/j.chembiol.2021.05.011.
65. Yesil P, Michel M, Chwalek K, Pedack S, Jany C, Ludwig B, Bornstein SR, and Lammert E (2009). A new collagenase blend increases the number of islets isolated from mouse pancreas. Islets 1, 185–190. 10.4161/isl.1.3.9556. [PubMed: 21099271]
66. Dobin A, Davis CA, Schlesinger F, Drenkow J, Zaleski C, Jha S, Batut P, Chaisson M, and Gingeras TR (2013). STAR: ultrafast universal RNA-seq aligner. Bioinformatics 29, 15–21. 10.1093/bioinformatics/bts635. [PubMed: 23104886]

67. Liao Y, Smyth GK, and Shi W (2013). The Subread aligner: fast, accurate and scalable read mapping by seed-and-vote. Nucleic Acids Res. 41, e108. 10.1093/nar/gkt214. [PubMed: 23558742]

68. Robinson MD, McCarthy DJ, and Smyth GK (2010). edgeR: a Bioconductor package for differential expression analysis of digital gene expression data. Bioinformatics 26, 139–140. 10.1093/bio-informatics/btp616. [PubMed: 19910308]

69. Hatakeyama M, Opitz L, Russo G, Qi W, Schlapbach R, and Rehrauer H (2016). SUSHI: an exquisite recipe for fully documented, reproducible and reusable NGS data analysis. BMC Bioinf. 17, 228. 10.1186/s12859-016-1104-8.

70. Schindelin J, Arganda-Carreras I, Frise E, Kaynig V, Longair M, Pietzsch T, Preibisch S, Rueden C, Saalfeld S, Schmid B, et al. (2012). Fiji: an open-source platform for biological-image analysis. Nat. Methods 9, 676–682. 10.1038/nmeth.2019. [PubMed: 22743772]

71. Arrivault S, Guenther M, Ivakov A, Feil R, Vosloh D, van Dongen JT, Sulpice R, and Stitt M (2009). Use of reverse-phase liquid chromatography, linked to tandem mass spectrometry, to profile the Calvin cycle and other metabolic intermediates in Arabidopsis rosettes at different carbon dioxide concentrations. Plant J. 59, 826–839. 10.1111/j.1365-313X.2009.03902.x. [PubMed: 19453453]

72. Shim SH, Lee SK, Lee DW, Brilhaus D, Wu G, Ko S, Lee CH, Weber APM, and Jeon JS (2019). Loss of function of rice plastidic glycolate/glycerate translocator 1 impairs photorespiration and plant growth. Front. Plant Sci. 10, 1726. 10.3389/fpls.2019.01726. [PubMed: 32038690]

73. Heinrich P, Kohler C, Ellmann L, Kuerner P, Spang R, Oefner PJ, and Dettmer K (2018). Correcting for natural isotope abundance and tracer impurity in MS-MS/MS- and high-resolution-multiple-tracer-data from stable isotope labeling experiments with IsoCorrectoR. Sci. Rep. 8, 17910. 10.1038/s41598-018-36293-4. [PubMed: 30559398]

74. Aplak E, von Montfort C, Haasler L, Stucki D, Steckel B, Reichert AS, Stahl W, and Brenneisen P (2020). CNP mediated selective toxicity on melanoma cells is accompanied by mitochondrial dysfunction. PLoS One 15, e0227926. 10.1371/journal.pone.0227926. [PubMed: 31951630]

Highlights

- Chronic insulin secretagogues increase islet viability but decrease secretory function
- Insulin secretagogues can enhance serine-linked mitochondrial one-carbon metabolism
- High-dose K_{ATP}-dependent insulin secretagogue DXO can deviate glucose flux to serine
- *Phgdh, Mthfd2*, and *Shmt2* limit insulin secretion but promote islet cell viability

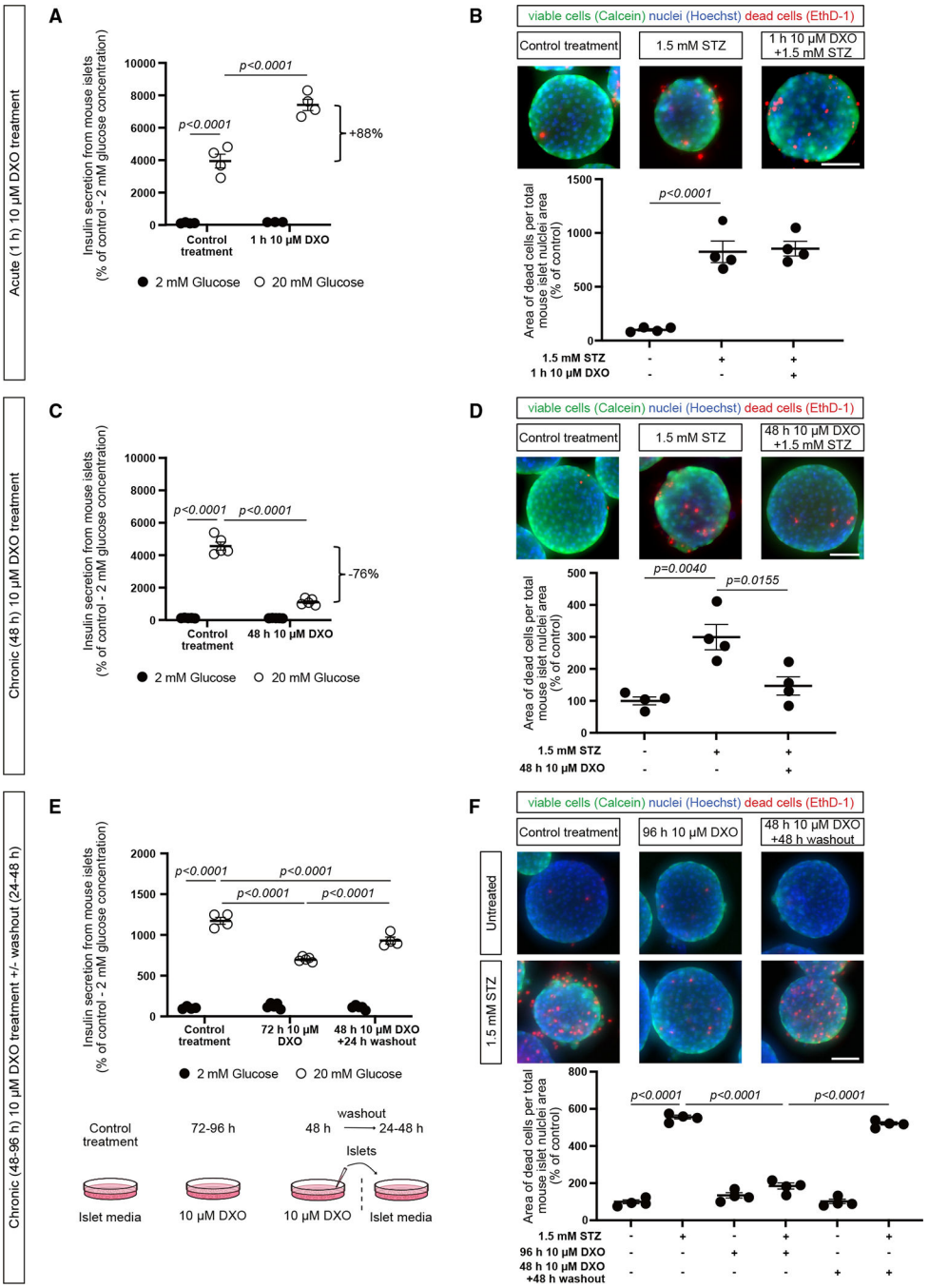

Figure 1. Insulin secretagogue DXO protects pancreatic islets from STZ-mediated cell death in a time-dependent and reversible manner, at the expense of their secretory function

(A) Insulin secretion from untreated and pre-treated mouse islets (1 h, 10 µM DXO) after low (2 mM) and high (20 mM) glucose stimulation. Reproduced in three independent experiments.

(B) Images and quantification of cell viability assay with mouse islets stained with ethidium homodimer-1 (EthD-1 for dead cells), calcein (for living cells), and Hoechst (for cell nuclei). Control treatment, no DXO or STZ; 1.5 mM STZ, no DXO followed by 24 h of 1.5 mM STZ; last panel, 1 h 10 µM DXO followed by 24 h of 1.5 mM STZ. Graph

represents quantification of islet images for non-viable cells. Reproduced in one independent experiment.

(C) Insulin secretion from untreated and pre-treated mouse islets (48 h, 10 μM DXO) after low (2 mM) and high (20 mM) glucose stimulation. Reproduced in six independent experiments.

(D) Images and quantification of cell viability assay with mouse islets stained with EthD-1 for dead cells, calcein and Hoechst. Control treatment, no DXO or STZ; 1.5 mM STZ, no DXO followed by 24 h of 1.5 mM STZ; last panel, 24 h of 10 μM DXO followed by 24 h 1.5 mM STZ and 10 μM DXO. Reproduced in four independent experiments.

(E) Insulin secretion from untreated mouse islets, mouse islets treated for 72 h with DXO, and mouse islets treated for 48 h with DXO followed by 24 h washout (transfer in normal culture medium) after low (2 mM) and high (20 mM) glucose stimulation. Reproduced in two independent experiments.

(F) Images and quantification of cell viability assay with mouse islets stained with EthD-1, calcein, and Hoechst. Untreated Control, no DXO or STZ; Untreated 96 h DXO, 96 h of 10 μM DXO and no STZ; Untreated 48 h DXO + 48 h washout, 48 h of 10 μM DXO followed by 48 h of no DXO and no STZ; 1.5 mM STZ Control, no DXO followed by 24 h of 1.5 mM STZ; 1.5 mM STZ 96 h DXO, 72 h of 10 μM DXO, followed by 24 h of DXO and 1.5 mM STZ; 1.5 mM STZ 48 h DXO + 48 h washout, 48 h of DXO, followed by 24 h washout, prior to 24 h of 1.5 mM STZ. Reproduced in two independent experiments. Scale bars, 50 μm. Please note that each dot in the insulin secretion panels represents an independent well containing seven or eight islets each, and data are depicted as mean ± SEM with corresponding p values and quantifications shown as percentage of control. Significance was determined by two-way ANOVA followed by Tukey's multiple comparison test (A, C, E) and one-way ANOVA followed by Dunnett's (B and D) or Tukey's multiple comparison test (F). See also Figure S1 for insulin contents and cell death validation, and Figure 3 for further washout experiments.

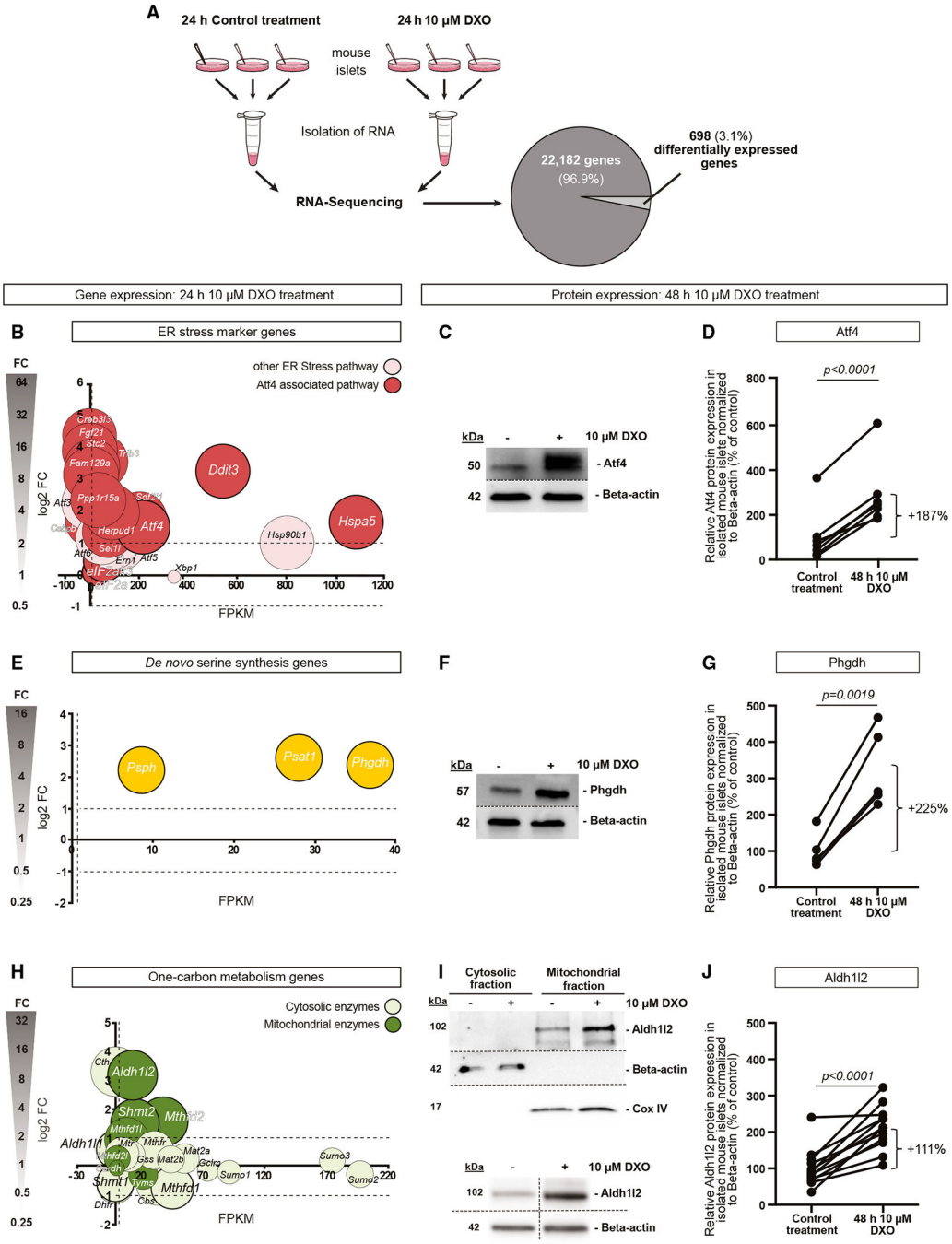

Figure 2. RNA-seq reveals upregulation of ER stress marker genes and genes encoding serine-linked mitochondrial OCM enzymes after chronic stimulation with DXO

(A) Schematic of RNA-seq setup. Genes, differentially expressed after treatment of islets with 10 μM DXO for 24 h (to observe the initial alterations in gene expression, followed by protein-based and functional analyses at 48 h), are shown on the pie chart. Change of expression was calculated as log2 fold change (log2 FC) with cutoff ≥ 1 and ≤ −1, p value <0.05, fragments per kilobase million (FPKM) >1.

(B) Expression analysis of ER stress marker genes.

(C and D) (C) Atf4 immunoblot of mouse pancreatic islets treated with 10 μM DXO for 48 h, and (D) quantification; n = 7 independent experiments.
(E) Expression analysis of genes encoding for enzymes of *de novo* serine synthesis.
(F and G) (F) Phgdh immunoblot of mouse islets treated with 10 μmM DXO for 48 h, and (G) quantification; n = 5 independent experiments.
(H) Expression analysis of genes encoding for enzymes involved in the mitochondrial and cytosolic OCM.
(I) Aldh1l2 immunoblot with fractionated (upper blot) and whole (lower blot) lysates of mouse islets treated with 10 μM DXO for 48 h.
(J) Quantification of whole-cell lysates; n = 12 independent experiments. Beta-actin was used for normalization. Graphs show genes and their log2 FC, FPKM, and p values based on RNA-seq data. The size of the circles is inversely proportional to the p value. Horizontal axes show FPKM values, vertical axes show log2 FC. Dashed lines indicate the restriction criteria of the FPKM and the log2 FC. Gradients on the left indicate the fold change. Genes of the Atf4 activated branch and cytosolic/mitochondrial serine-linked OCM are highlighted by larger font size. All quantifications of blots are shown as percentage of control, and significance was determined by two-tailed paired Student's t test (D, G, J). See also Figures S2A–S2D for islet cell and proliferation marker gene expression levels.

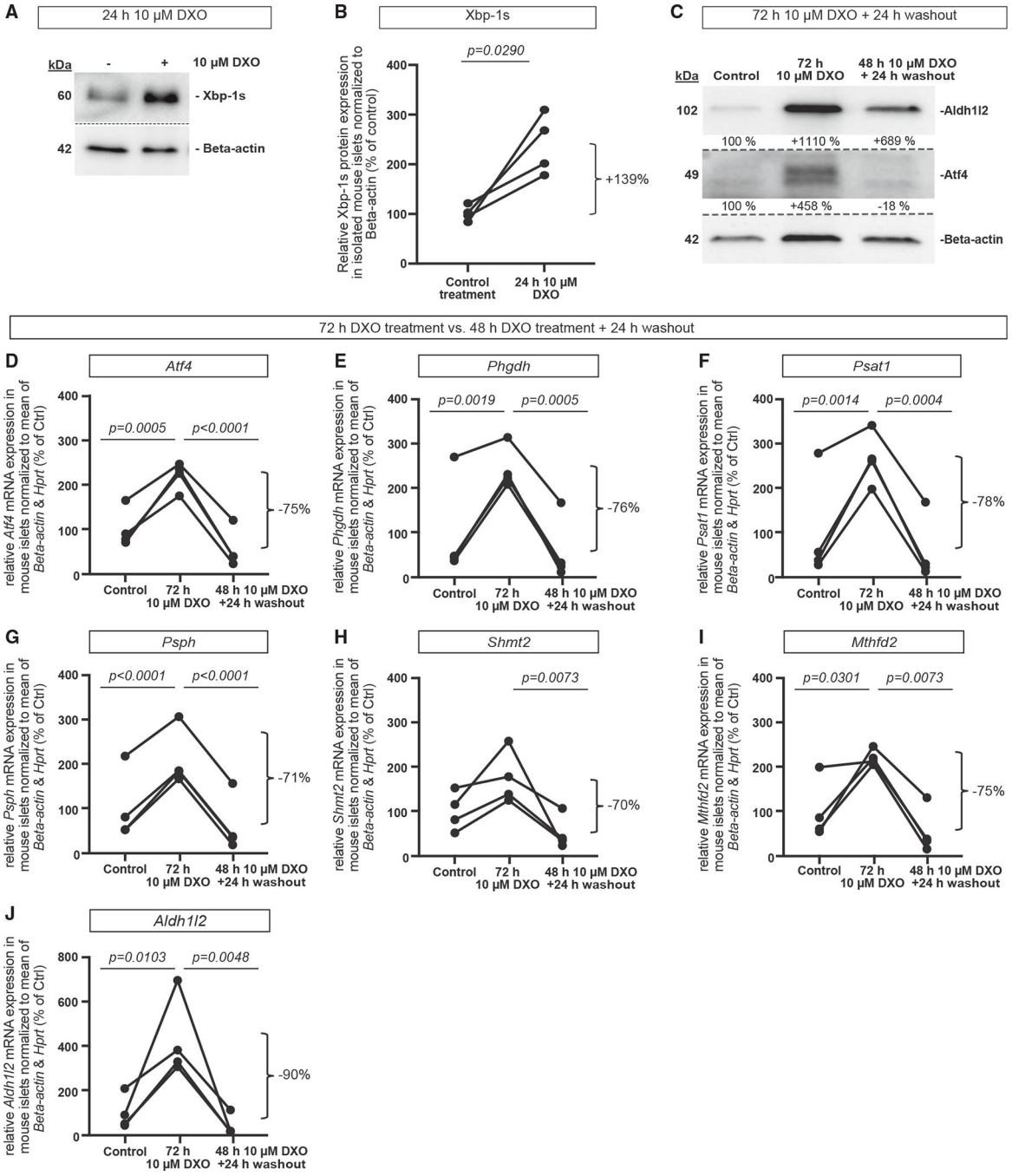

Figure 3. Chronic stimulation of islets with DXO induces Xbp-1s protein expression and reversibly increases serine-linked mitochondrial OCM gene expression

(A) Immunoblot for Xbp-1s (a marker of unfolded protein response, UPR in brief) in islets after treatment with 10 µM DXO for 24 h.

(B) Quantification of Xbp-1s normalized to Beta-actin; n = 4 independent treatments.

(C–J) Islets were left untreated (control), treated with 10 µM DXO for 72 h, or treated with 10 µM DXO for 48 h followed by 24 h washout. (C) Immunoblot for Aldh1l2, Atf4, and Beta-actin in lysates from pancreatic islets. Reproduced in five independent experiments.

(D–J) Relative mRNA expression of (D) *Atf4*, (E) *Phgdh*, (F) *Psat1*, (G) *Psph*, (H) *Shmt2*,

(I) *Mthfd2*, and (J) *Aldh1l2*, in pancreatic islets. n = 4 independent experiments. Data are shown as mean ± SEM with corresponding p values and quantifications shown as percentage of control. Statistical significance was determined by two-tailed paired Student's t test (B) and one-way ANOVA followed by Tukey's multiple comparison test (D–J).

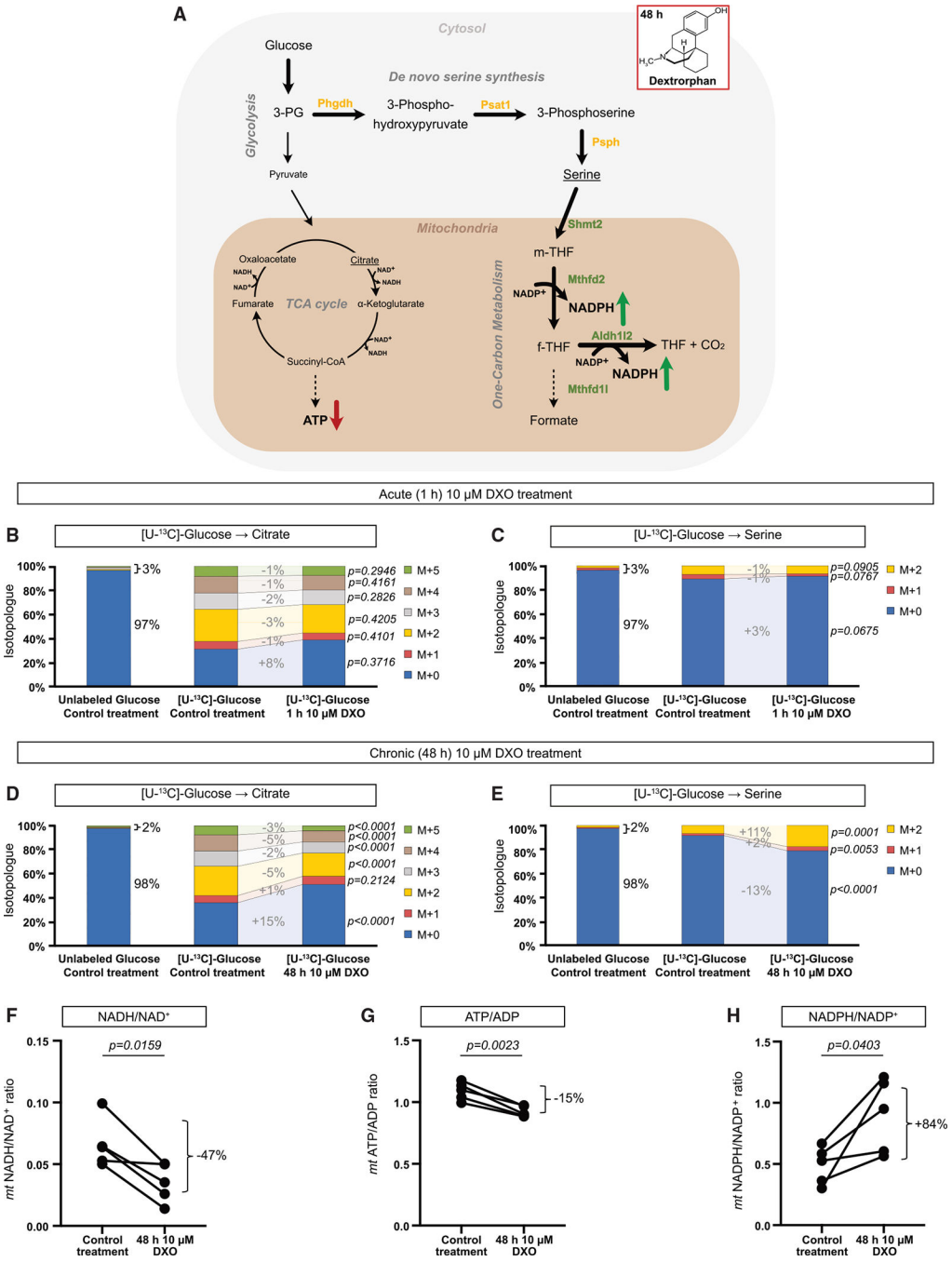

Figure 4. Chronic stimulation of islets with a high dose of DXO deviates the glucose flux into the serine-linked mitochondrial OCM

(A) Schematic of the proposed mechanism by which treatment of islets with 10 μM DXO for 48 h (mimicking “chronic,” high-dose drug treatment) induces islet cell protection against STZ-mediated cell death at the expense of insulin secretory function. The serine-linked mitochondrial OCM is represented on the scheme only by the enzymes significantly upregulated by the treatment. Bold arrows indicate reactions catalyzed by enzymes upregulated upon chronic treatment with a high dose of the insulin secretagogue DXO. 3-PG, 3-phosphoglycerate; ATP, adenosine triphosphate; NAD^+/NADH,

nicotinamide adenine dinucleotide; $NADP^+$/NADPH, nicotinamide adenine dinucleotide phosphate; TCA cycle, tricarboxylic acid cycle; Succinyl-CoA, succinyl-coenzyme A; Phgdh, phosphoglycerate dehydrogenase; Psat1, phosphoserine aminotransferase 1; Psph, phosphoserine phosphatase; Shmt2, serine hydroxy methyltransferase 2; Mthfd2, methylenetetrahydrofolate dehydrogenase 2; Aldh1l2, aldehyde dehydrogenase 1 family member L2; Mthfd1l, methylenetetrahydrofolate dehydrogenase 1-like; m-THF, methyl-THF; f-THF, formyl-THF; THF, 5,6,7,8-tetrahydrofolate; CO_2, carbon dioxide.

(B–E) Metabolic tracing of U-^{13}C-glucose in mouse islets treated for 1 h (B and C) or 48 h (D and E) with or without the insulin secretagogue DXO. Measurement of ^{13}C incorporation into the TCA cycle intermediate citrate (B and D) and the *de novo* serine synthesis product serine (C and E). Please note that, during fragmentation, citrate (C_6 body) and serine (C_3 body) lost one C atom each. Quantification was performed based on pool of n = 3 (B and C) and n = 4 (D and E) independent experiments.

(F–H) (F) Mitochondrial NADH/NAD^+, (G) ATP/ADP, and (H) NADPH/$NADP^+$ ratios in pancreatic islets treated with 10 μM DXO for 48 h. n = 5 independent experiments. All quantifications are shown as percentage of control and significance was determined by two-tailed unpaired (B–E) and paired Student’s t test (F–H).

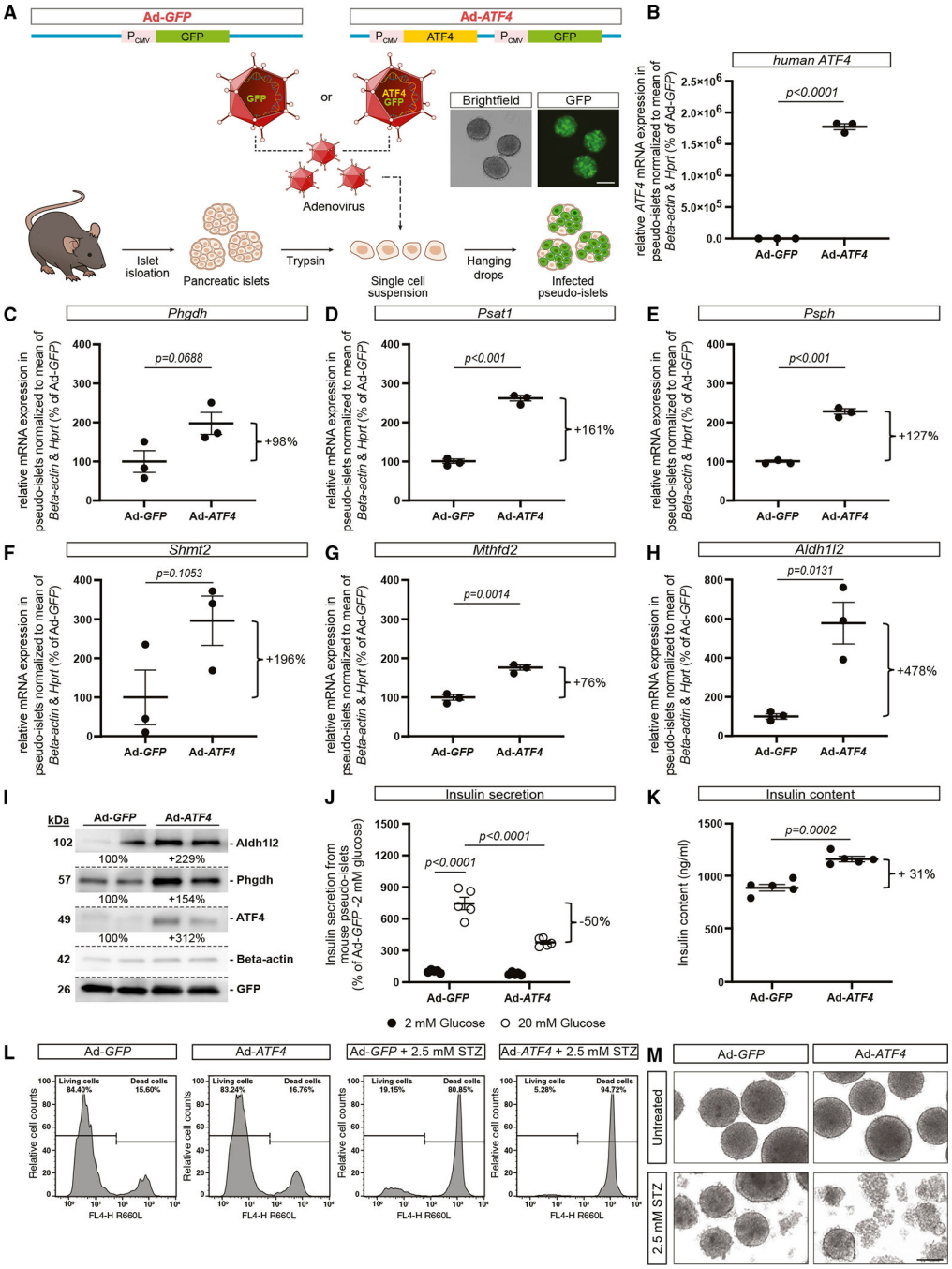

Figure 5. Overexpression of human ATF4 in islets enhances gene expression levels of serine-linked mitochondrial OCM enzymes and decreases GSIS

(A) Scheme of adenoviral GFP (Ad-*GFP*) and human *ATF4* (Ad-*ATF4*) plasmid transduction into dispersed mouse islet cells and subsequent generation of pseudo-islets. Representative images of pseudo-islets infected with Ad-*GFP*. Scale bar, 100 μm. (B–H) Relative mRNA expression of (B) human *ATF4*, (C) *Phgdh*, (D) *Psat1*, (E) *Psph*, (F) *Shmt2*, (G) *Mthfd2*, and (H) *Aldh1l2* in pseudo-islets infected with Ad-*GFP* or Ad-*ATF4*. Reproduced in one (C and E) and three (D and F–H) independent experiments.

(I) Immunoblot of Aldh1l2, Phgdh, ATF4, Beta-actin, and GFP in pseudo-islets infected with Ad-*GFP* as control or Ad-*ATF4*. Relative protein expression was normalized to GFP expression levels. Reproduced in two independent experiments.
(J) Insulin secretion of Ad-*GFP* and Ad-*ATF4* infected pseudo-islets, after low (2 mM) and high (20 mM) glucose stimulation. Reproduced in two independent experiments.
(K) Insulin content of infected pseudo-islets. Reproduced in two independent experiments.
(L) Flow cytometry analysis of cell viability using FVS660. Histograms of Ad-*GFP* or Ad-*ATF4* infected mouse islet cells, demonstrating live (FL4-H negative) and dead (FL4-H positive) cell populations after treatment with 2.5 mM STZ for 24 h. Reproduced in two independent experiments.
(M) Bright-field images of infected pseudo-islets after 24 h of 2.5 mM STZ treatment. Scale bar, 100 μm. Please note that each dot in the insulin secretion and content panels represents an independent well containing seven or eight islets each, and data are presented as mean ± SEM with corresponding p values and quantifications shown as percentage of Ad-*GFP* control. Statistical significance was evaluated by two-tailed unpaired Student's t test (B–H and K) or two-way ANOVA followed by Tukey's multiple comparison test (J).

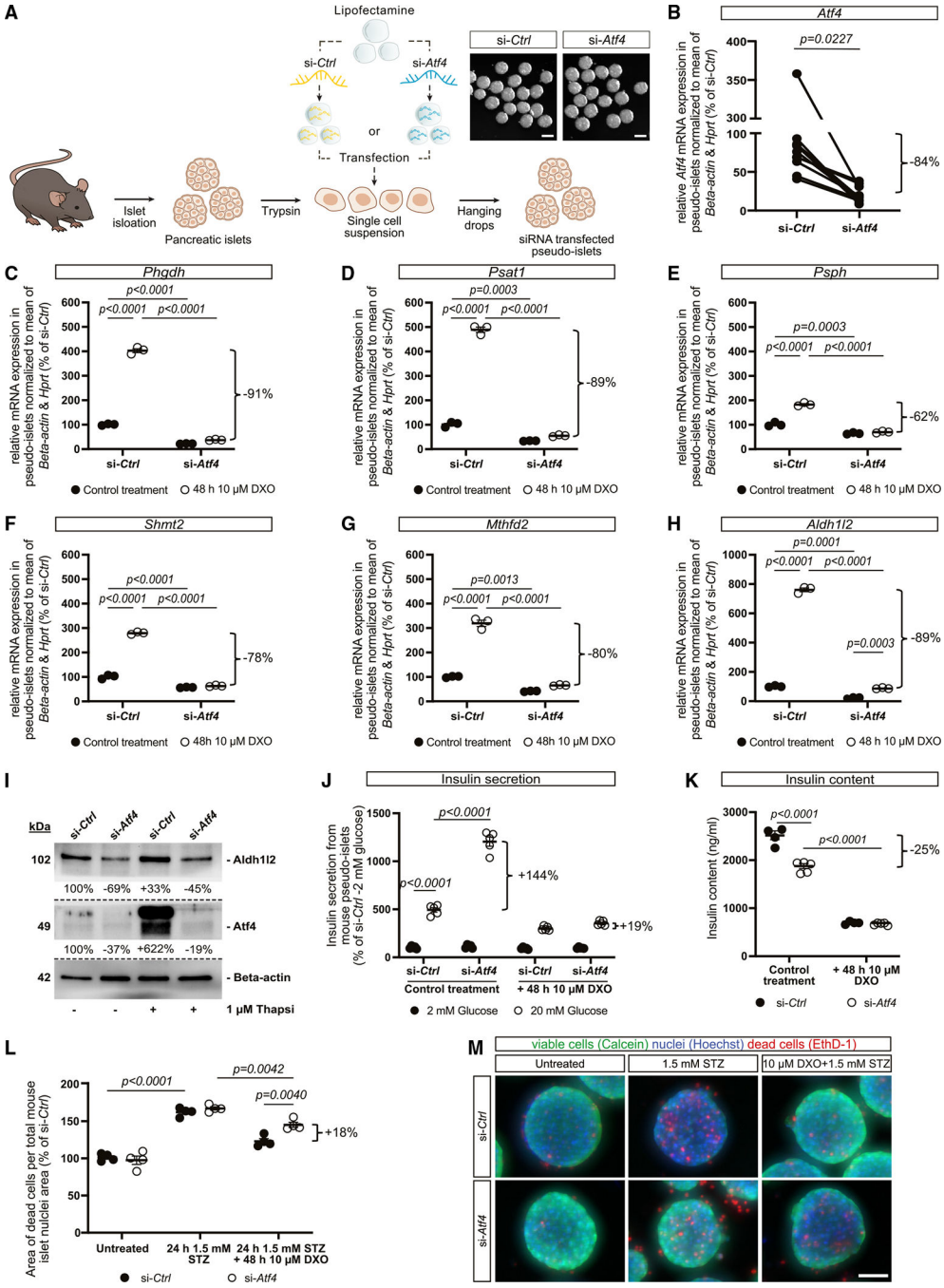

Figure 6. Knockdown of *Atf4* in pseudo-islets attenuates DXO-induced upregulation of serine-linked mitochondrial OCM genes, enhances GSIS, and prevents full DXO-mediated islet protection from STZ-mediated cell death

(A–H) (A) Experimental setup for siRNA-mediated knockdown of *Atf4* (si-*Atf4*) in dispersed mouse islet cells and generation of pseudo-islets. Scale bar, 100 µm. Relative mRNA expression of (B) *Atf4* (n = 10) in control siRNA (si-Ctrl) and si-*Atf4* transfected pseudo-islets, and relative mRNA levels of the enzymes (C) *Phgdh*, (D) *Psat1*, (E) *Psph*, (F) *Shmt2*, (G) *Mthfd2*, and (H) *Aldh1l2* in transfected pseudo-islets with or without 10 µM DXO for 48 h. Reproduced in three (G) and seven (C–F and H) independent experiments.

(I) Immunoblot of Aldh1l2, Atf4, and Beta-actin in siRNA-transfected pseudo-islets that were either untreated or treated with 1 μM ER stressor thapsigargin (Thapsi) for 24 h. Beta-actin was used as a loading control. Reproduced in one independent experiment.
(J) Insulin secretion of siRNA-transfected pseudo-islets treated with or without 10 μM DXO for 48 h, after low (2 mM) and high (20 mM) glucose stimulation. Reproduced in three independent experiments.
(K) Insulin content in transfected pseudo-islets treated with or without 10 μM DXO for 48 h. Reproduced in three independent experiments.
(L and M) (L) Quantification and (M) images of cell viability assays with siRNA-transfected pseudo-islets stained with EthD-1, calcein and Hoechst. Untreated, no DXO or STZ; 24 h 1.5 mM STZ, no DXO, followed by 24 h of 1.5 mM STZ; 10 μM DXO + 1.5 mM STZ, 24 h of 10 μM DXO, followed by 24 h of 1.5 mM STZ and 10 μM DXO. Scale bar, 50 μm. Please note that each dot in the insulin secretion and content panels represents an independent well containing seven or eight islets each; data are presented as mean ± SEM with corresponding p values, and quantifications are shown as percentage of untreated si-*Ctrl*. Statistical significance was determined by two-tailed paired Student's t test (B) and two-way ANOVA, followed by Tukey's multiple comparison test (C–H and J–L).

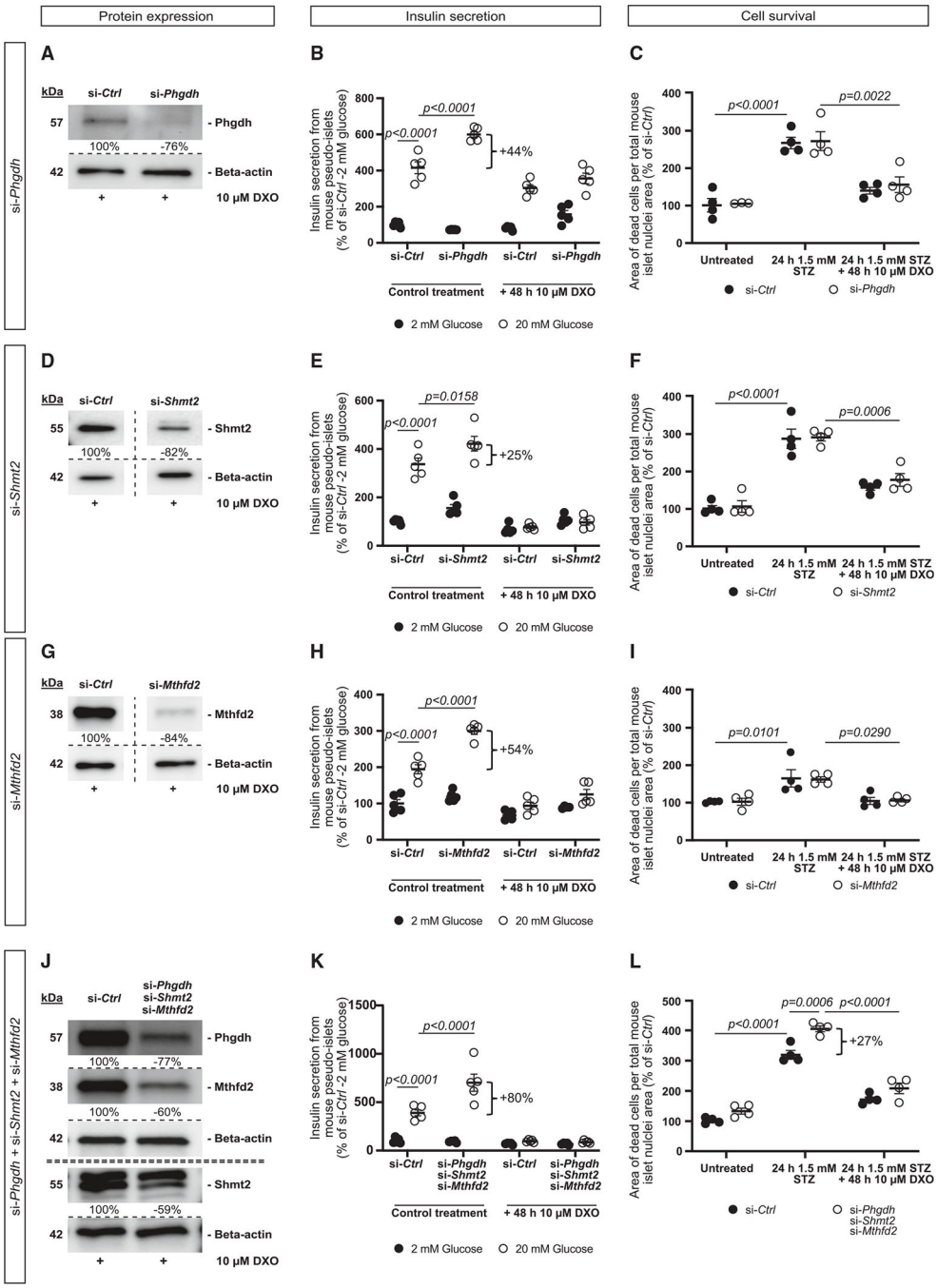

Figure 7. Single knockdown of serine-linked mitochondrial OCM genes *Phgdh, Shmt2*, and *Mthfd2* enhances GSIS, while triple knockdown reduces protection of pseudo-islets from STZ-mediated cell death

(A) Immunoblot of Phgdh in si-*Ctrl*- and si-*Phgdh*-siRNA-transfected pseudo-islets confirms the knockdown of the enzyme, with Beta-actin used as loading control. Reproduced in three independent experiments.

(B) Insulin secretion of untreated and pre-treated (48 h, 10 μM DXO) siRNA-transfected pseudo-islets, after low (2 mM) and high (20 mM) glucose stimulation. Reproduced in two independent experiments.

(C) Quantification of cell viability assay with untreated or 24 h 10 μM DXO pre-treated siRNA-transfected pseudo-islets, prior to additional 24 h with 1.5 mM STZ.
(D) Immunoblot of Shmt2 in si-*Ctrl*- and si-*Shmt2*-transfected pseudo-islets. Reproduced in one independent experiment.
(E) Insulin secretion of untreated and pre-treated (48 h, 10 μM DXO) siRNA-transfected pseudo-islets, after low (2 mM) and high (20 mM) glucose stimulation.
(F) Quantification of cell viability assay with untreated or 24 h 10 μM DXO pre-treated siRNA-transfected pseudo-islets, prior to additional 24 h with 1.5 mM STZ. Reproduced in one independent experiment.
(G) Immunoblot of Mthfd2 in si-*Ctrl*- and si-*Mthfd2*-transfected pseudo-islets. Reproduced in two independent experiments.
(H) Insulin secretion of untreated and pre-treated (48 h, 10 μM DXO) siRNA-transfected pseudo-islets, after low (2 mM) and high (20 mM) glucose stimulation. Reproduced in two independent experiments.
(I) Quantification of cell viability assay with untreated 24 h 10 μM DXO pre-treated siRNA-transfected pseudo-islets, prior to additional 24 h with 1.5 mM STZ. Reproduced in two independent experiments.
(J) Immunoblot of Phgdh, Shmt2, and Mthfd2 in si-*Ctrl*- and si-*Phgdh* + si-*Shmt2* + si-*Mthfd2*-transfected pseudo-islets. Reproduced in one independent experiment.
(K) Insulin secretion of untreated and pre-treated (48 h, 10 μM DXO) siRNA-transfected pseudo-islets, after low (2 mM) and high (20 mM) glucose stimulation.
(L) Quantification of cell viability assay with untreated or 24 h 10 μM DXO pre-treated siRNA-transfected pseudo-islets, prior to additional 24 h with 1.5 mM STZ. Please note that each dot in the insulin secretion panels represents an independent well containing seven or eight islets each; data are presented as mean ± SEM with corresponding p values, and quantifications are shown as percentage of untreated si-*Ctrl*. Statistical significance was determined by two-way ANOVA followed by Tukey's multiple comparison test.

KEY RESOURCES TABLE

REAGENT or RESOURCE	SOURCE	IDENTIFIER
Antibodies		
See Table S1_Antibodies	This paper; See Table S1	See Table S1
Bacterial and virus strains		
Adenovirus: Ad-GFP control (Ad-*GFP*)	ViraQuest Inc	VQAd CMV eGFP
Adenovirus: Ad-human ATF4 (Ad-*ATF4*)	Vector Biolabs	Cat#ADV-201618; RefSeq: BC011994
Chemicals, peptides, and recombinant proteins		
(+)-MK-801 hydrogen maleate	Sigma-Aldrich	Cat#M107
[U-^{13}C]-Glucose	Sigma-Aldrich	Cat#389374
Dextromethorphan hydrobromide monohydrate (DXM)	Sigma-Aldrich	Cat#D2531
Dextrorphan tartrate (DXO)	Sigma-Aldrich	Cat#D127
Exendin-4	Sigma-Aldrich	Cat#E7144
Glibenclamide	Abcam	Cat#ab120267
Lipofectamine RNAiMAX	Thermo Fisher Scientific	Cat#13778-150
Streptozotocin	Sigma-Aldrich	Cat#S0130
Thapsigargin	Sigma-Aldrich	Cat#T9033
Critical commercial assays		
LUNA® Universal qPCR Master Mix	NEB	Cat#M3003E
SuperScript™ II reverse transcriptase Kit	Invitrogen by Thermo Fisher Scientific	Cat#18064071
High-Capacity cDNA Reverse Transcription Kit	Invitrogen by Thermo Fisher Scientific	Cat#4368813
Mitochondria/Cytosol Fractionation Kit	Abcam	Cat#ab65320
RNase-Free DNase Set	Qiagen	Cat#79254
RNeasy Mini Kit	Qiagen	Cat#74104
Ultra-sensitive rat insulin ELISA Kit	Crystal Chem	Cat#90062
Deposited data		
RNA-sequencing raw and analyzed data	This paper; Mendeley Data	DOI:10.17632/4rwmrc9cpr.4 and DOI: 10.17632/g4bdvw6czr.2
Experimental models: Organisms/strains		
Mouse: C57BL/6JRj	Janvier Labs	https://www.janvier-labs.com/en/fiche_produit/c57bl-6jrj_mouse/; RRID: MGI:5897683
Mouse: C57BL/6NTac	Taconic	https://www.taconic.com/mousemodel/black-6-b6ntac
Mouse: BKS(D)-*Leprdb*/JOrlRj	Janvier Labs	https://janvier-labs.com/fiche_produit/diabetique-souris/

REAGENT or RESOURCE	SOURCE	IDENTIFIER
Mouse: Fluorescent beta cell reporter strain: B6(Cg)-Ins1$^{tm1.1(cre)Thor}$/J × B6.Cg-Gt(ROSA)26Sor$^{tm9(CAG-tdTomato)Hze}$/J	In-house intercross of published and commercially available (Jackson Laboratories, USA) mouse strains	https://www.jax.org/strain/007909; RRID: IMSR_JAX:007909 https://www.jax.org/strain/026801; RRID: IMSR_JAX:026801
Oligonucleotides		
See Table S2_Oligonucleotides	This paper, See Table S2	See Table S2
Software and algorithms		
Code for pancreatic islet analyses of cell viability	Scholz et al.[64]; Zenodo	https://doi.org/10.5281/zenodo.5820007
Fiji (ImageJ) image analysis software	Schindelin et al.[70]	RRID: SCR_002285
FlowJo V10	BD Biosciences	RRID: SCR_008520
GraphPad Prism	GraphPad Software	RRID: SCR_002798
Other		
Fixable viability stain 660	BD Biosciences	Cat#564405
Hoechst 33342	Thermo Fisher Scientific	Cat#H3570
LIVE-DEAD viability-cytotoxicity Kit	Thermo Fisher Scientific	Cat#L3224